arXiv:1007.2032v1 [astro-ph.SR] 13 Jul 2010

SUB-Alfvénic NON-IDEAL MHD TURBULENCE SIMULATIONS WITH AMBIPOLAR DIFFUSION: II. COMPARISON WITH OBSERVATION, CLUMP PROPERTIES, AND SCALING TO PHYSICAL UNITS

Christopher F. McKee
Physics Department and Astronomy Department, University of California, Berkeley, CA 94720; and Laboratoire d'Etudes du Rayonnement et de la Matière en Astrophysique, LERMA-LRA, Ecole Normale Superieure, 24 rue Lhomond, 75005 Paris, France

Pak Shing Li
Astronomy Department, University of California, Berkeley, CA 94720

and

Richard I. Klein
Astronomy Department, University of California, Berkeley, CA 94720; and Lawrence Livermore National Laboratory, P.O.Box 808, L-23, Livermore, CA 94550
Draft version July 14, 2010

ABSTRACT

Ambipolar diffusion is important in redistributing magnetic flux and in damping Alfvén waves in molecular clouds. The importance of ambipolar diffusion on a length scale ℓ is governed by the ambipolar diffusion Reynolds number, $R_{\rm AD} = \ell/\ell_{\rm AD}$, where $\ell_{\rm AD}$ is the characteristic length scale for ambipolar diffusion. The logarithmic mean of the AD Reynolds number in a sample of 15 molecular clumps with measured magnetic fields (Crutcher 1999) is 17, comparable to the theoretically expected value. We identify several regimes of ambipolar diffusion in a turbulent medium, depending on the ratio of the flow time to collision times between ions and neutrals; the clumps observed by Crutcher (1999) are all in the standard regime of ambipolar diffusion, in which the neutrals and ions are coupled over a flow time. We have carried out two-fluid simulations of ambipolar diffusion in isothermal, turbulent boxes for a range of values of $R_{\rm AD}$. The mean Mach numbers were fixed at $\mathcal{M} = 3$ and $\mathcal{M}_{\rm A} = 0.67$; self-gravity was not included. We study the properties of overdensities–i.e., clumps– in the simulation and show that the slope of the higher-mass portion of the clump mass spectrum increases as $R_{\rm AD}$ decreases, which is qualitatively consistent with Padoan et al. (2007)'s finding that the mass spectrum in hydrodynamic turbulence is significantly steeper than in ideal MHD turbulence. For a value of $R_{\rm AD}$ similar to the observed value, we find a slope that is consistent with that of the high-mass end of the Initial Mass Function for stars. However, the value we find for the spectral index in our ideal MHD simulation differs from theirs, presumably because our simulations have different initial conditions. This suggests that the mass spectrum of the clumps in the Padoan et al. (2007) turbulent fragmentation model for the IMF depends on the environment, which would conflict with evidence for a universal IMF. In addition, we give a general discussion of how the results of simulations of magnetized, turbulent, isothermal boxes can be scaled to physical systems. Each physical process that is introduced into the simulation, such as ambipolar diffusion, introduces a dimensionless parameter, such as $R_{\rm AD}$, which must be fixed for the simulation, thereby reducing the number of scaling parameters by one. We show that the importance of self-gravity is fixed in any simulation of ambipolar diffusion; it is not possible to carry out a simulation in which self-gravity and ambipolar diffusion are varied independently unless the ionization is a free parameter. We show that our simulations apply to small regions in molecular clouds, generally with $\ell_0 \lesssim 0.4$ pc and $M \lesssim 25\ M_\odot$. A general discussion of the scaling relations for magnetized, isothermal, turbulent boxes, including self-gravitating systems, is given in the Appendix.

Subject headings: Magnetic fields—MHD—ISM: magnetic fields—ISM: kinematics and dynamics—stars:formation

1. INTRODUCTION

Giant molecular clouds, threaded by magnetic fields, are the birth places for new stars. Since the earliest studies of star formation, it has been recognized that the magnetic flux in stars is many orders of magnitude less than that in the interstellar material from which the stars originated. Mestel & Spitzer (1956) suggested that ambipolar diffusion (AD) could resolve this prob-

cmckee@astro.berkeley.edu
psli@astron.berkeley.edu
klein@astron.berkeley.edu

lem by allowing magnetic flux to be redistributed during collapse due to the differential motion between the ionized and neutral gas. With effective shielding of high energy cosmic rays and radiation, the ionization fraction of gas inside high-density cloud cores can be $\leq 10^{-7}$ (e.g. Caselli et al. 1998; Bergin et al. 1999), which renders AD efficient. Star formation theory based on the AD-regulated, quasi-static collapse of molecular clouds (e.g. Spitzer 1968; Nakano & Tademaru 1972; Mouschovias 1976, 1977, 1979; Nakano & Nakamura 1978; Shu 1983; Lizano & Shu 1989; Fiedler & Mouschovias 1992, 1993)

naturally accounts for the enormous loss of magnetic flux during star formation.

However, both observations (Zuckerman & Evans 1974; Zuckerman & Palmer 1974) and theory (Arons & Max 1975) have long indicated that supersonic turbulent motions are important in molecular clouds, and this turbulence has a major effect on star formation (Mac Low & Klessen 2004; Ballesteros-Paredes et al. 2007; McKee & Ostriker 2007). The kinetic energy of the supersonic motions is observed to be comparable to the magnetic energy of the clouds, so that molecular clouds are in approximate equipartition (e.g. Crutcher 1999; Heiles & Troland 2005; Troland & Crutcher 2008). It should be borne in mind that the amplitude of turbulent fluctuations decreases with decreasing scale; for example, Goodman et al. (1998) and Barranco & Goodman (1998) find that the NH_3 lines within ~ 0.1 pc of the centers of the cores that they examined do not obey the line width-size relations as seen on the large scale (e.g. Larson 1981; Solomon et al. 1987; Heyer & Brunt 2004). Mouschovias (1987) and Myers & Lazarian (1998) have argued that AD would damp turbulent motions on small scales, and Goodman et al. (1998) suggest that this damping could be enhanced by the low ionization fraction in the dense inner regions of the cores. Better data will enable determination of the role of ambipolar diffusion on the small scales relevant to the formation of individual stars. Existing data clearly show that turbulence is important on larger scales, but observational tests of the theoretical prediction that turbulence can accelerate the rate of AD (Fatuzzo & Adams 2002; Zweibel 2002) will be challenging.

Numerical simulation is an important tool in understanding supersonic turbulence in magnetized MCs, but it is very challenging to carry out three-dimensional (3D) simulations that include ambipolar diffusion. The small ionization fraction in molecular clouds means that the ion inertia can be neglected. This permits a single-fluid treatment of ambipolar diffusion, which gives the induction equation the form of a diffusion equation (e.g. Mac Low et al. 1995; Duffin & Pudritz 2008). However, in this case the the stability condition for explicit codes requires the time step to scale as the square of the grid-size (Δx^2 —Mac Low et al. 1995), which is prohibitive at high resolution (e.g. Nakamura & Li 2008). Li, McKee, & Klein (2006; hereafter LMK) developed the Heavy-Ion Approximation, which takes advantage of the negligible ion inertia in regions of very low ionization and can accelerate simulations of ambipolar diffusion by large factors. In the Heavy-Ion Approximation, the mass-weighted ionization is increased by a factor $\mathcal{R} \sim 10^4$ and the ion-neutral coupling coefficient is decreased by the same factor, so that the momentum transfer between ions and neutrals is unaffected. Using a semi-implicit two-fluid scheme proposed by Mac Low & Smith (1997) (see also Tóth 1995), LMK tested the Heavy-Ion Approximation with several classical problems involving ambipolar diffusion and found speed-ups of order a factor 100.

In the first astrophysical application of the Heavy-Ion Approximation, Li et al (2008, hereafter LMKF) studied the statistical properties of supersonically turbulent systems with ambipolar diffusion. The properties of the turbulence were found to vary smoothly from the hydrodynamic case to the ideal MHD case as the importance of ambipolar diffusion decreased. They found that the power spectra for the neutral gas properties of a strongly magnetized medium with strong ambipolar diffusion are similar to those for a weakly magnetized medium; in particular, the power spectrum for the neutral velocity is close to that for Burger's turbulence.

In this paper, we extend this work on turbulent systems with ambipolar diffusion but without self-gravity. This paper has three main goals: First, we give a general discussion of the ambipolar diffusion Reynolds number, R_{AD}, that characterizes ambipolar diffusion (Myers & Khersonsky 1995; Zweibel 2002) (§2). We then determine the numerical values of R_{AD} for the molecular regions studied by Crutcher (1999) (§2) and show that they are consistent with the theoretically expected ones. Second, we use numerical simulations to determine the properties of the clumps that appear in a turbulent medium with ambipolar diffusion (§§3 & 4). In particular, we show how the mass function and the mass-to-flux ratio of the clumps depend on R_{AD}. Third, we analyze the scaling properties of simulations with ambipolar diffusion and determine the range of physical parameters that characterize the simulations (§5). This discussion is continued in the Appendix, which gives a general discussion of how the results of simulations of turbulent boxes can be applied to physical systems, including those that are self-gravitating. Further results from these simulations, particularly those relevant to measuring the strength of the magnetic field and determining the effects of heating due to ambipolar diffusion, will be discussed in a future paper (Paper III).

2. THE AMBIPOLAR DIFFUSION REYNOLDS NUMBER

The effects of ambipolar diffusion on a length scale ℓ in a medium with a flow velocity v can be characterized by the ambipolar diffusion (AD) Reynolds number, $R_{AD}(\ell)$. This quantity appears to have been first introduced by Myers & Khersonsky (1995); they referred to it as the magnetic Reynolds number, although that term is normally used to describe the effects of Ohmic resistivity. The AD Reynolds number is motivated as follows (Zweibel & Brandenburg 1997; Zweibel 2002, LMK): Ions in a partially ionized plasma are subject to two forces: the Lorentz force, $\sim B_{rms}^2/4\pi\ell_B$, where B_{rms} is the rms magnetic field strength and $\ell_B \equiv |B_{rms}/\nabla B_{rms}|$; and the drag force, $\gamma_{AD}\rho_i\rho_n v_{AD}$, where γ_{AD} is the ion-neutral coupling coefficient, ρ_i and ρ_n are the ion and neutral densities, respectively, and v_{AD} is the drift velocity between the neutrals and the ions. When the ionization is low enough that the ion inertia can be neglected, these forces balance and the drift velocity is

$$v_{AD}(\ell_B) \simeq \frac{B_{rms}^2}{4\pi\gamma_{AD}\rho_i\rho_n\ell_B}. \tag{1}$$

We define the ambipolar-diffusion time over a length scale ℓ as

$$t_{AD}(\ell) \equiv \frac{\ell}{v_{AD}(\ell)} = \frac{4\pi\gamma_{AD}\rho_i\rho_n\ell^2}{B_{rms}^2}. \tag{2}$$

Similarly, we can introduce the ambipolar-diffusion length scale ℓ_{AD}, which is the length for which the ambipolar drift velocity is the same as the flow velocity— i.e., in the frame of the ions, the length scale over which

the field varies in a steady flow:

$$\ell_{\mathrm{AD}} = \frac{B_{\mathrm{rms}}^2}{4\pi\gamma_{\mathrm{AD}}\rho_i\rho_n v}. \qquad (3)$$

In terms of the neutral-ion collision time, $t_{ni} = 1/\gamma_{\mathrm{AD}}\rho_i$, the AD time scale and length scale are

$$t_{\mathrm{AD}} = \frac{\ell^2}{v_{\mathrm{A}}^2 t_{ni}}, \qquad (4)$$

$$\ell_{\mathrm{AD}} = \frac{v_{\mathrm{A}}^2 t_{ni}}{v}, \qquad (5)$$

where $v_{\mathrm{A}} = B_{\mathrm{rms}}/(4\pi\rho)^{1/2}$ is the Alfvén velocity and where we have assumed that the ion mass density is negligible, so that $\rho_n \simeq \rho$. The effect of ambipolar diffusion on a flow over a length scale ℓ with a characteristic velocity v is determined by the AD Reynolds number,

$$R_{\mathrm{AD}}(\ell) \equiv \frac{\ell v}{v_A^2 t_{ni}} = \frac{t_{\mathrm{AD}}}{t_f} = \frac{\ell}{\ell_{\mathrm{AD}}} = \frac{4\pi\gamma_{\mathrm{AD}}\bar{\rho}_i\bar{\rho}_n\ell v}{B_{\mathrm{rms}}^2}, \quad (6)$$

where $t_f \equiv \ell/v$ is the flow time across a length ℓ. Observe that ambipolar diffusion increases in importance as $R_{\mathrm{AD}}(\ell)$ decreases; thus, it becomes more important at low densities, low ionizations, low velocities, small distances and high field strengths. As Myers & Khersonsky (1995) showed, the ratio of the size of the region, ℓ, to the minimum wavelength of a propagating Alfvén wave in which the inertia is provided by the neutrals , $\lambda_{\min} = \pi v_{\mathrm{A}} t_{ni}$ (Kulsrud & Pearce 1969), is directly proportional to $R_{\mathrm{AD}}(\ell)$:

$$\frac{\ell}{\lambda_{\min}} = \frac{R_{\mathrm{AD}}(\ell)}{\pi\mathcal{M}_{\mathrm{A}}}, \qquad (7)$$

where $\mathcal{M}_{\mathrm{A}} \equiv v/v_{\mathrm{A}}$ is the Alfvén Mach number.

We have defined the AD Reynolds number in terms of the mean densities and the rms field strength. In a supersonically turbulent medium, the densities are subject to large fluctuations, and if the Alfvén Mach number is large also, the magnetic field has large fluctuations as well. If one defines R_{AD} in terms of the local densities and field strength, then one can devise several different ways of averaging so as to obtain an effective value of R_{AD} for a turbulent medium; in particular, the length scale ℓ can be taken to be the size of the region or it can be determined self-consistently as the size of the average eddy or density fluctuation. The resulting values for R_{AD} in a turbulent region of size ℓ_0 range from slightly larger than $R_{\mathrm{AD}}(\ell_0)$ to several times less (see Paper III for further discussion). One should thus bear in mind that $R_{\mathrm{AD}}(\ell_0)$ is a characteristic value for the ratio of the ambipolar diffusion time to the flow time, and the actual value in a turbulent medium might differ from this by a factor of a few.

Mouschovias (private communication) has emphasized that the AD Reynolds number is useful for turbulent media in which the velocity dispersion is determined by the turbulence (the case we are considering here), but not in systems in which the flow velocity is determined by the AD process itself. For example, in quasi-static, AD-regulated star formation, the AD length scale, ℓ_{AD} is proportional to the radius of the self-gravitating cloud, and R_{AD} is of order unity. Similarly, R_{AD} is not a useful

parameter to characterize C-shocks (Draine 1980), since the structure of such shocks adjusts itself so that $R_{\mathrm{AD}} \sim 1$ (Li, McKee, & Klein 2006).

2.1. Numerical Evaluation of $R_{\mathrm{AD}}(\ell)$

Evaluation of the AD Reynolds number requires evaluation of both the ion-neutral coupling coefficient, γ_{AD}, and of the mean ionization mass fraction, $\bar{\chi}_i \equiv \bar{\rho}_i/\bar{\rho}$. If this mass fraction is small ($\bar{\chi}_i \ll 1$), then $\bar{\rho}_n \simeq \bar{\rho}$ and

$$R_{\mathrm{AD}}(\ell) = \frac{1}{2}\left(\frac{\gamma_{\mathrm{AD}}\bar{\rho}\ell}{c_s}\right)\bar{\chi}_i\mathcal{M}\beta = \left(\frac{\gamma_{\mathrm{AD}}\bar{\rho}\ell}{c_s}\right)\frac{\bar{\chi}_i\mathcal{M}_{\mathrm{A}}^2}{\mathcal{M}},$$

$$(8)$$

where c_s is the isothermal sound speed, $\mathcal{M} \equiv v/c_s$ is the Mach number and $\beta \equiv 8\pi\bar{\rho}c_s^2/B_{\mathrm{rms}}^2$ is the plasma β parameter. We normalize our results to the case in which the ionization is dominated by HCO^+. The ion-neutral coupling coefficient is then

$$\gamma_{\mathrm{AD}} = \frac{1.9 \times 10^{-9}\ \mathrm{cm}^3\ \mathrm{s}^{-1}}{m_n + m_i} = 3.7 \times 10^{13}\ \mathrm{cm}^3\ \mathrm{s}^{-1}\ \mathrm{g}^{-1}$$

$$(9)$$

(Draine, Roberge, & Dalgarno 1983), provided the relative velocity of the ions and neutrals is less than about 19 km s^{-1}. Note that this value of the coupling coefficient differs from that adopted in LMKF due to our assumption that the ionization is dominated by HCO^+. More generally, we shall write

$$\gamma_{\mathrm{AD}} = 3.7 \times 10^{13}\gamma_{\mathrm{AD}}{}^*\ \mathrm{cm}^3\ \mathrm{s}^{-1}\ \mathrm{g}^{-1}, \qquad (10)$$

where $\gamma_{\mathrm{AD}}{}^*$ is a number that allows for ions other than HCO^+.

Next, we consider the ionization. The processes that determine the ionization in molecular clouds are complex, and in general the ionization is time-dependent. We adopt a characteristic value of the ionization based on the assumption that the ionization is in a steady state and is dominated by HCO^+. In equilibrium, the mean ionization fraction by number is

$$\bar{x}_{e,\,\mathrm{eq}} = \left(\frac{\zeta_{\mathrm{CR}}}{\alpha\bar{n}_{\mathrm{H}}}\right)^{1/2}, \qquad (11)$$

where $\bar{n}_{\mathrm{H}} = \bar{\rho}/\mu_{\mathrm{H}}$ is the mean density of H nuclei, $\mu_{\mathrm{H}} = 2.34 \times 10^{-24}$ g is the mass per H nucleus, $\zeta_{\mathrm{CR}} \sim 3 \times 10^{-17}$ s^{-1} is the cosmic ray ionization rate per H atom (see the discussion by Dalgarno 2006) and α is the relevant recombination rate (McKee & Ostriker 2007). Equation (11) is consistent with the results of Padoan et al. (2004) at late times and high densities for $\alpha = 2.5 \times 10^{-6}$ cm^3 s^{-1}, the value they adopted for the dissociative recombination rate of HCO^+. If small PAHs dominate the ionization, then the dissociative recombination rate is about 10 times smaller (Wakelam & Herbst 2008) and the ionization several times larger. Tassis & Mouschovias (2005, 2007), who included the effects of charged grains, adopted a dissociative recombination rate $\alpha = 1.0 \times 10^{-6}$ cm^3 s^{-1}; their results for the ionization are approximately consistent with equation (11) for densities $n_{\mathrm{H}} \lesssim 10^8$ cm^{-3}.

Inference of the ionization from observations generally requires knowledge of the cosmic ray ionization rate and the density as inputs to the chemical models

used to interpret the observations (Williams et al. 1998; Padoan et al. 2004). The ionization can be characterized by the parameter C_i defined by

$$x_e \equiv C_i \left(\frac{\zeta_{\mathrm{CR}}}{n_{\mathrm{H}}} \right)^{1/2}. \qquad (12)$$

In the equilibrium model above, $C_i = \alpha^{-1/2}$, which is 630 cm$^{3/2}$ s$^{1/2}$ for the fiducial case. Williams et al. (1998) found a median ionization $x_e = 4.5 \times 10^{-8}$ (note that they normalized their results to H$_2$, whereas we are normalizing with respect to H). Their adopted ionization rate ($\zeta_{\mathrm{CR}} = 2.5 \times 10^{-17}$ s^{-1}) and density ($n_{\mathrm{H}} = 5 \times 10^4$ cm^{-3}) correspond to $C_i \simeq 2000$ cm$^{3/2}$ s$^{1/2}$. More recently, Padoan et al. (2004) have interpreted these data with time dependent models and infer lower values of the ionization and therefore C_i. They find $x_e \simeq 7.5 \times 10^{-9} - 3.5 \times 10^{-8}$ and attribute the higher values to the effect of FUV photoionization; for their assumed ionization rate ($\zeta_{\mathrm{CR}} = 6 \times 10^{-18}$ s^{-1}) and density (2×10^4 cm^{-3}), the implied value of the ionization parameter is $C_i \sim 600$ cm$^{3/2}$ s$^{1/2}$, fortuitously close to our fiducial value. The difference between the values of C_i inferred by Williams et al. (1998) and Padoan et al. (2004) is a reflection of the uncertainties that remain in determining the ionization in molecular clouds.

To evaluate the AD Reynolds number, we require the ion *mass* fraction $\bar{\chi}_i$, which is related to the ion number fraction $\bar{x}_i \equiv \bar{n}_i/\bar{n}_{\mathrm{H}}$ by $\bar{\chi}_i = \bar{x}_i m_i/\mu_{\mathrm{H}} \to 20.7\bar{x}_i$, where the numerical evaluation is for HCO$^+$. We then have

$$\bar{\chi}_i = \frac{m_i C_i}{\mu_{\mathrm{H}}} \left(\frac{\zeta_{\mathrm{CR}}}{\bar{n}_{\mathrm{H}}} \right)^{1/2} = 2.25 \times 10^{-6} \left(\frac{\chi_i^*}{\bar{n}_{\mathrm{H},3}^{1/2}} \right), \quad (13)$$

where the numerical factor

$$\chi_i^* = \frac{m_i}{29 \text{ amu}} \left(\frac{C_i}{630 \text{ cm}^{3/2} \text{ s}^{1/2}} \right) \left(\frac{\zeta_{\mathrm{CR}}}{3 \times 10^{-17} \text{ s}^{-1}} \right)^{1/2} \qquad (14)$$

allows for deviations from the fiducial case and where $\bar{n}_{\mathrm{H},3} \equiv \bar{n}_{\mathrm{H}}/(10^3 \text{ cm}^{-3})$. Under the assumption that the ion mass is indeed about 29 amu (i.e., the mass of HCO$^+$), the results of Williams et al. (1998) correspond to $\chi_i^* \simeq 3$, whereas those of (Padoan et al. 2004) correspond to $\chi_i^* \simeq 1$. The ionization can also be expressed in the form $\rho_i = \mathcal{C}\rho^{1/2}$ (Shu 1983), with $\mathcal{C} = \chi_i \rho^{1/2} = 1.09 \times 10^{-16}\chi_i^*$ g$^{1/2}$ cm$^{-3/2}$. Shu (1983) adopted a value $\mathcal{C} = 3 \times 10^{-16}$ g$^{1/2}$, corresponding to $\chi_i^* \sim 3$, in agreement with the estimate of Williams et al. (1998). Numerically, the AD Reynolds number is then

$$R_{\mathrm{AD}}(\ell) = 16.0\gamma_{\mathrm{AD}}^*\chi_i^*\mathcal{M}\beta \left(\frac{\bar{n}_{\mathrm{H},3}^{1/2}\ell_{\mathrm{pc}}}{T_1^{1/2}} \right), \qquad (15)$$

where $T_1 \equiv T/(10 \text{ K})$ and $\ell_{\mathrm{pc}} \equiv \ell/(1 \text{ pc})$.

2.2. *Regimes of Ambipolar Diffusion*

We can distinguish several regimes in ambipolar diffusion in a turbulent medium. For $\chi_i \equiv \rho_i/\rho \ll 1$, we have $\rho_n \simeq \rho$ so that the neutral-ion collision time, t_{ni} and the corresponding ion-neutral collision time, t_{in} are related

by

$$t_{in} \equiv \frac{1}{\gamma_{\mathrm{AD}}\rho_n} = \frac{\chi_i}{\gamma_{\mathrm{AD}}\rho_i} = \chi_i t_{ni}. \qquad (16)$$

Similarly, the ion-Alfvén Mach number, $\mathcal{M}_{\mathrm{A}i} \equiv v(4\pi\rho_i)^{1/2}/B_{\mathrm{rms}}$, is related to the Alfvén Mach number, $\mathcal{M}_{\mathrm{A}}$, by $\mathcal{M}_{\mathrm{A}i}^2 = \chi_i\mathcal{M}_{\mathrm{A}}^2$. It follows that

$$R_{\mathrm{AD}} = \mathcal{M}_{\mathrm{A}}^2 \left(\frac{t_f}{t_{ni}} \right) = \mathcal{M}_{\mathrm{A}i}^2 \left(\frac{t_f}{t_{in}} \right). \qquad (17)$$

We now identify five different regimes for ambipolar diffusion. For simplicity we ignore possible differences between the velocity dispersions of the neutrals and ions (to be discussed in Paper III), which could change the coefficient in front of $\mathcal{M}_{\mathrm{A}i}^2$ by up to a factor 2 in the expressions below.

I. Ideal MHD ($t_f/t_{ni} \to \infty$, corresponding to $R_{\mathrm{AD}} \to \infty$ for a given value of $\mathcal{M}_{\mathrm{A}}$): The ions and neutrals are perfectly coupled.

II. Standard AD ($t_f > t_{ni} \gg t_{in}$, corresponding to $R_{\mathrm{AD}} > \mathcal{M}_{\mathrm{A}}^2$): The neutrals and ions are coupled together over a flow time so that the AD is weak. For $\mathcal{M}_{\mathrm{A}} = \mathcal{O}(1)$, linear Alfvén waves can propagate, since the propagation condition for Alfvén waves of wavelength ℓ derived by Kulsrud & Pearce (1969) is equivalent to $R_{\mathrm{AD}}(\ell) > \pi\mathcal{M}_{\mathrm{A}}$ (eq. 7). The wave damping is weak (i.e., $\Gamma t_f < 1$, where $\Gamma = \frac{1}{2}k^2v_{\mathrm{A}}^2 t_{ni}$ is the damping rate for low-frequency waves) for $R_{\mathrm{AD}}(\ell) > 2\pi^2$.

III. Strong AD ($t_{ni} > t_f > t_{in}$, corresponding to $\mathcal{M}_{\mathrm{A}}^2 > R_{\mathrm{AD}} > \mathcal{M}_{\mathrm{A}i}^2$): The neutrals are no longer coupled to the ions in a flow time, but the ions remain coupled to the neutrals. For $\mathcal{M}_{\mathrm{A}} = \mathcal{O}(1)$, Alfvén waves cannot propagate since $\lambda_{\mathrm{min}}/\ell > \pi/\mathcal{M}_{\mathrm{A}} \gtrsim 1$ (eq. 7).

IV. Weakly coupled ($t_{in} > t_f$, corresponding to $\mathcal{M}_{\mathrm{A}i}^2 > R_{\mathrm{AD}}$): The ions and neutrals are only weakly coupled and act almost independently. The damping rate for the high-frequency Alfvén waves that propagate in the ions is $\Gamma = 1/(2t_{in})$, so these waves are weakly damped in this regime: $\Gamma t_f = R_{\mathrm{AD}}(\ell)/(2\mathcal{M}_{\mathrm{A}i}^2) < 1$ for waves of wavelength ℓ. The Heavy-Ion Approximation is based on the assumption that the ion inertia is negligible and therefore does not apply to this regime (see below).

V. Hydrodynamics ($t_f/t_{in} \to 0$ or $\chi_i \to 0$, corresponding to $R_{\mathrm{AD}} \to 0$ for a given value of $\mathcal{M}_{\mathrm{A}}$): The neutrals are not affected by the trace ions and act purely hydrodynamically. One can of course recover the hydrodynamic limit by letting $B \to 0$ so that $\mathcal{M}_{\mathrm{A}} \to \infty$; in that case, R_{AD} is unconstrained. It should be noted that the boundary between the hydrodynamic regime and the weakly coupled regime is a matter of choice; if one demands that the ions have at most a 1% effect on the neutrals, for example, then R_{AD} would have to be smaller than if one demands that the effects be limited to 10%.

It should be borne in mind that in all regimes except the last (where it is irrelevant), we have assumed that the ions are well-coupled to the magnetic field—i.e., the ion gyrofrequency is much larger than the ion-neutral collision frequency, $\Omega_i t_{in} \gg 1$. Although we have defined the AD regimes for arbitrary values of the Alfvén Mach number (provided B is large enough that $\Omega_i t_{in} \gg 1$), this characterization of ambipolar diffusion is most useful when $\mathcal{M}_A \sim \mathcal{O}(1)$, as it generally is in molecular gas in the interstellar medium.

2.3. Observed Values of R_{AD}

Crutcher (1999) has summarized sensitive Zeeman measurements of magnetic field strengths together with other physical parameters, including the plasma β and the Mach numbers, for 27 molecular clouds. Of these, 12 have only an upper limit on the line-of-sight magnetic field. Table 1 lists the values of the parameters from Tables 1 and 2 in Crutcher (1999) that we use to compute the corresponding R_{AD} using equation (15). We take the length scale ℓ_0 to be the cloud diameter. We use Crutcher's correction for projection effects on the magnetic field: Zeeman observations determine the line-of-sight component of the field, B_{los}, and on average the value of B^2 that enters the plasma-β parameter is $3B_{los}^2$. We assume that the parameters describing the ion-neutral coupling and the ionization ($\gamma_{AD}{}^*$ and χ_i^*) are unity. From Table 1, we see that clouds with measured field strengths have R_{AD} ranging from a few to ~ 70. Because the range of R_{AD} is so large, we quote the logarithmic average, defined as

$$\langle R_{AD} \rangle_{\log} \equiv 10^{\langle \log R_{AD} \rangle}; \qquad (18)$$

the logarithmic mean and dispersion of the AD Reynolds number in these clouds is $\langle R_{AD} \rangle_{\log} = 17 \pm 0.4$ dex. Clouds that have only upper limits on the magnetic field have an average lower limit on the AD Reynolds number of $\langle R_{AD} \rangle_{\log} = 22$; if we discard L889 as an outlier because of its unusually high Mach number ($\mathcal{M} = 7.3$), the logarithmic mean is 18, which is comparable to that of the clouds with measured fields. We also include the Alfvén Mach number, $\mathcal{M}_A$, in Table 1. All the clouds have $R_{AD} > \mathcal{M}_A{}^2$, implying that these clouds are in the standard AD regime (§2.2). The ratio of the size of the cloud to the minimum Alfvén wavelength is in the range $2 - 15$ for clouds with measured field strengths. We conclude that the effects of ambipolar diffusion must be considered in studies of molecular clouds, at least in those regions shielded from the interstellar radiation field so that $\chi_i^* = \mathcal{O}(1)$, in agreement with studies extending back for many years (e.g., Mouschovias 1987).

2.4. Predicted R_{AD} and Implied Self-Gravity

As we now show, it is possible to predict the AD Reynolds number for self-gravitating clouds that have an ionization of the form given in equation (13). As a corollary, we show that the strength of self-gravity is not a free parameter in simulations of ambipolar diffusion in a turbulent medium.

The importance of self-gravity in a cloud of radius R_0 or in a simulation box of size $\ell_0 = 2R_0$ is determined by

the virial parameter (Bertoldi & McKee 1992),

$$\alpha_{vir} \equiv \frac{5\sigma^2 R_0}{GM_0} = \frac{5\sigma^2 \ell_0}{2GM_0}, \qquad (19)$$

where

$$\sigma = \frac{1}{\sqrt{3}}\, \mathcal{M} c_s \qquad (20)$$

is the 1D velocity dispersion in the cloud. The virial parameter is thus proportional to the ratio of kinetic to gravitational energy. We wish to treat both real clouds, which we approximate as effectively spherical, and turbulent boxes. Of course, real clouds are not spherical (Bertoldi & McKee 1992 give the generalization to elliptical clouds), but keeping track of these two cases provides a gauge of the importance of geometric effects; furthermore, the spherical cloud model has long been in use (e.g., Solomon et al. 1987). Let the area and volume of the cloud or box be

$$A \equiv c_A \ell_0^2, \qquad (21)$$
$$V \equiv c_V \ell_0^3, \qquad (22)$$

where $c_A = (\pi/4, 1)$ and $c_V = (\pi/6, 1)$ for a spherical cloud and a box, respectively. The virial parameter then becomes

$$\alpha_{vir} = \frac{5\mathcal{M}^2 c_s^2}{6 c_V G \bar{\rho} \ell_0^2}. \qquad (23)$$

Since $\bar{\rho}_i \equiv \bar{\chi}_i \bar{\rho}$, equation (8) for the AD Reynolds number can be rewritten as

$$R_{AD}(\ell_0) = \left(\frac{5}{6 c_V G \alpha_{vir}} \right)^{1/2} \gamma_{AD} \bar{\chi}_i \bar{\rho}^{1/2} \mathcal{M}_A{}^2, \qquad (24)$$

which shows that the AD Reynolds number is determined by the ionization, the Alfvén Mach number and the virial parameter. Insofar as the ionization is a function of the density, $R_{AD}(\ell_0)$ will also depend on density. However, in the case of greatest interest, in which $\bar{\chi}_i \propto \chi_i^* \bar{\rho}^{-1/2}$, where χ_i^* is a number that is unity in the fiducial case (eq. 14), the AD Reynolds number is fixed at

$$R_{AD}(\ell_0) = 19.7 \gamma_{AD}{}^* \chi_i^* \left(\frac{\pi}{6 c_V \alpha_{vir}} \right)^{1/2} \mathcal{M}_A{}^2. \qquad (25)$$

Molecular cloud cores and clumps with measured magnetic fields are typically self-gravitating, with $\alpha_{vir} \sim 1$, and have $\mathcal{M}_A \sim 1$ (Crutcher 1999). As a result, for the fiducial values of γ_{AD} and χ_i, such regions have $R_{AD}(\ell) \sim 20$. This predicted value is in good agreement with the observed values discussed in §2.3, which have a logarithmic mean of 17 and a dispersion of 0.4 dex. GMCs as a whole have larger values of $R_{AD}(\ell)$ since most of their mass is photoionized by UV radiation (McKee 1989), so that they have a higher ionization than the cores and clumps within them (e.g., in an envelope of a GMC in which the ionization is dominated by C^+, the ionization parameter is $\chi_i^* \sim 10^2$).

The importance of self-gravity in a magnetized medium can also be expressed in terms of the ratio of the mass to the magnetic critical mass, M_Φ, which is the minimum mass that can undergo gravitational collapse. In terms

of the magnetic flux, $\Phi \equiv B c_A \ell_0^2$, the magnetic critical mass is

$$M_\Phi = c_\Phi \frac{\Phi}{G^{1/2}} \ , \qquad (26)$$

where $c_\Phi = 1/2\pi$ for a cold sheet (Nakano & Nakamura 1978) and ≈ 0.12 for a cloud with a flux-to-mass distribution corresponding to a uniform field threading a uniform spherical cloud (Mouschovias & Spitzer 1976; Tomisaka et al. 1988). For $c_\Phi = 1/2\pi$, the ratio of the mass to the magnetic critical mass is

$$\mu_{\Phi,0} \equiv \frac{M_0}{M_\Phi} = \left(\frac{5\pi c_V}{6 c_A^2 \alpha_{\rm vir}}\right)^{1/2} \mathcal{M}_A \qquad (27)$$

$$\rightarrow \left(\frac{20}{9}\right)^{1/2} \frac{\mathcal{M}_A}{\alpha_{\rm vir}^{1/2}} \qquad \text{(spherical cloud)} (28)$$

which provides a simple relation between the Alfvén Mach number, $\mathcal{M}_A$ and the two parameters describing the importance of self gravity in a magnetized, turbulent cloud, $\alpha_{\rm vir}$ and $\mu_{\Phi,0}$. The ratio $\mu_{\Phi,0}$ is sometimes written as the ratio of the observed mass-to-flux ratio to the critical one, $(M/\Phi)_{\rm obs}/(M/\Phi)_{\rm crit}$ (e.g., Troland & Crutcher 2008). Using equation (25), we find that the AD Reynolds number is given in terms of $\mu_{\Phi,0}$ by

$$R_{\rm AD}(\ell_0) = 13.2 \left(\frac{2c_A}{3c_V}\right) \gamma_{\rm AD}{}^* \chi_i^* \mathcal{M}_A \mu_{\Phi,0}; \qquad (29)$$

the factor in parentheses is unity for a spherical cloud. Gravitationally bound clouds that are both magnetized and turbulent have $\mu_{\Phi,0}$ somewhat greater than unity since the gravity has to overcome both the turbulent motions and the magnetic field (McKee 1989). This expression thus gives a similar result to that in equation (25) for $\mathcal{M}_A \sim 1$ and $\mu_{\phi,0} \simeq 1 - 2$.

These relations for $R_{\rm AD}(\ell_0)$ can be inverted to give the values of the virial parameter and the ratio of the mass to the critical mass in terms of $R_{\rm AD}(\ell_0)$ and $\mathcal{M}_A$. In other words, a simulation of a turbulent box with ambipolar diffusion [which requires specification of $R_{\rm AD}(\ell_0)$ and $\mathcal{M}_A$] necessarily implies the strength self-gravity would have were it to be included:

$$\alpha_{\rm vir} = 203 \left[\frac{\gamma_{\rm AD}{}^* \chi_i^*}{R_{\rm AD}(\ell_0)}\right]^2 \mathcal{M}_A{}^4 \ , \qquad (30)$$

$$\mu_{\Phi,0} = 0.114 \left[\frac{R_{\rm AD}(\ell_0)}{\gamma_{\rm AD}{}^* \chi_i^*}\right] \frac{1}{\mathcal{M}_A} \ , \qquad (31)$$

where we have set $c_A = c_V = 1$, as is appropriate for a simulation box. For $\alpha_{\rm vir} \gg 1$, the neglect of self-gravity is self-consistent. Parameter choices that lead to values of $\alpha_{\rm vir} \ll 1$ and $\mu_{\Phi,0} \gtrsim 1$ are not self-consistent, since self-gravity would lead to turbulent motions that render $\alpha_{\rm vir} \gtrsim 1$ (e.g., Klessen & Hennebelle 2009).

We emphasize that "implied self gravity" does not mean that simulations of ambipolar diffusion mimic the effects of self gravity. Rather, it means that the strength of the self-gravity, were it to be included, is not a free parameter provided the ionization parameter χ_i^* is specified.[1] By contrast, a simulation of a turbulent box with

ideal MHD is scale free; the density can be chosen so that self-gravity would be negligible if it were included. This freedom does not exist in simulations of ambipolar diffusion.

3. SIMULATIONS

In this paper, we extend the LMKF study of supersonic turbulence with ambipolar diffusion, focusing on the physical properties of the clumps formed purely as the result of turbulent fragmentation with no gravity. LMKF performed a series of 256^3 simulations in a periodic box using the code ZEUS-MPAD to investigate turbulence statistics in non-ideal MHD without self-gravity. Like LMKF, we drove the turbulence with a fixed driving pattern over the wavenumber range $1 \leq k \leq 2$ (where $k \equiv k_{\rm phys}\ell_0/2\pi = \ell_0/\lambda$ is the normalized wavenumber) using the recipe described in Mac Low (1999). The driving maintained the 3D Mach number at $\mathcal{M} = 3$, which is only mildly supersonic. The corresponding line-of-sight Mach number—i.e., the 1D Mach number $\mathcal{M}/\sqrt{3}$—is less than 2. The magnetic field was initially uniform, with a strength set by a plasma-β parameter of 0.1, corresponding to an Alfvén Mach number $\mathcal{M}_A = 0.67$; the turbulence is thus sub-Alfvénic. During the simulations, the volume-averaged magnetic field changed by less than 10%, and as a result the volume-averaged value of β remained within 10% of its initial value. As shown in Table 1, this value of β is close to the median of the 15 clouds with measured magnetic fields.

The focus of our effort is to determine how the properties of the clumps vary with $R_{\rm AD}(\ell_0)$, so for now we discuss our results in dimensionless form; the physical conditions corresponding to these simulations will be discussed in §5 below. We note, however, that for systems satisfying the linewidth-size relation, a Mach number of 3 corresponds to a box size $\ell_0 \simeq 0.4$ pc. Like LMKF, we considered values of $R_{\rm AD}(\ell_0)$ from 0.12, close to the hydrodynamic limit, to 1200, close to the ideal MHD limit. The run with $R_{\rm AD}(\ell_0) = 12$ has conditions similar to those in observed clouds; as we shall see below, if we assume that the simulated region satisfies the linewidth-size relation, its density would be $\bar{n}_{\rm H} \simeq 10^4$ cm^{-3}. In §4.2.1, we show that the inertial range of the simulated turbulence extends over the range $\ell_0/3 - \ell_0/20$, so the AD length scale $\ell_{\rm AD} = \ell_0/R_{\rm AD}(\ell_0)$ is in the inertial range for this run. For all the other runs, the AD length scale is outside the inertial range. The run with $R_{\rm AD}(\ell_0) = 1.2$ focuses on scales less than $\ell_{\rm AD}$ and has a lower value of the AD Reynolds number than any of the clouds observed by Crutcher (1999), most of which are gravitationally bound. If the simulation satisfied the linewidth-size relation, it would have a density of $\bar{n}_{\rm H} \simeq 400$ cm^{-3}, corresponding to an unbound cloud. On the other hand, the runs with $R_{\rm AD}(\ell_0) = 120, 1200$ focus on scales greater than $\ell_{\rm AD}$ and have higher AD Reynolds numbers than any of the clouds with measured magnetic fields in that sample. The $R_{\rm AD}(\ell_0) = 1200$ run could be applied to the outer parts of GMCs, where the ionization is dominated by C^+. The run with $R_{\rm AD}(\ell_0) = 0.12$ represents the

---

[1] Of course, the relation between $\alpha_{\rm vir}$ and $R_{\rm AD}(\ell_0)$ also depends on $\mathcal{M}_A$, but this is fixed in simulations of turbulent boxes with $\mathcal{M}_A \lesssim 1$; by contrast, whereas observed clouds have definite values of χ_i^*, it is not necessary to specify this quantity in the simulation—see §A.3.

transition to the hydrodynamic limit, and is primarily of theoretical rather than practical interest.

All models were run for $3t_f$, where $t_f \equiv \ell_0/\mathcal{M}c_s$ is the flow time. In order to improve the statistics and the resolution, we re-ran the five models m3c2r-1 [$R_{AD}(\ell_0) = 0.12$] to m3c2r3 [$R_{AD}(\ell_0) = 1200$; see Table 2] in LMKF with the same initial conditions but using a 512^3 grid. All the results reported in this paper are the result of simulations on such a grid. The total computing time for all the models was $\sim 600,000$ CPU hours on the NCSA machine Abe using 512 processors.

We made two principal approximations in our simulations. First, as discussed in the Introduction, we used the Heavy Ion Approximation (LMK), adopting an ionization $\tilde{\chi}_{i0} = \mathcal{R}\chi_{i0}$ and a corresponding ion-neutral coupling coefficient $\tilde{\gamma}_{AD} \propto \gamma_{AD}/\mathcal{R}$, with $\mathcal{R} \sim 10^4$; here the tilde denotes quantities measured in code units (see §A.3). The key to the Heavy Ion Approximation is that even though each of these parameters differs from the actual value by a factor of 10^4, the ion-neutral coupling is governed by the product of the parameters and has the correct physical value. According to the discussion in §2.2, the five AD models and the ideal MHD model span three regimes of AD as listed in Table 2, based on the initial $R_{AD}(\ell_0)$ in equilibrium.

Our second principal approximation was in our treatment of the ionization. Simulations can be carried out with various assumptions about the ionization, including ion conservation, ionization equilibrium and time-dependent ionization. Following LMKF, we assumed that the number of ions is conserved, so that the value of $\bar{\chi}_i$ for the entire box is constant. The density is initially uniform, so that the initial ionization mass fraction, $\bar{\chi}_{i0}$, is the same everywhere; we took it to be 10^{-6}. LMKF demonstrated that the results were the same as in the case of ionization equilibrium (basically because the time for a neutral to exchange momentum with an ion is small compared to the ionization time scale). More generally, the ionization is time-dependent. The ratio of the flow time, $t_f \equiv \ell_0/\mathcal{M}c_s$, to the characteristic ionization time, $t_{\rm ion,eq} = x_{e,\rm eq}/\zeta_{\rm CR}$ (see eq. 11), is large:

$$\frac{t_f}{t_{\rm ion,eq}} = (\alpha\zeta_{\rm CR}\bar{n}_{\rm H})^{1/2}\left(\frac{\ell_0}{\mathcal{M}c_s}\right), \qquad (32)$$

$$= 1.40 \times 10^3 (\alpha^* \zeta_{\rm CR}^*)^{1/2}\left[\frac{R_{AD}(\ell_0)}{\gamma_{AD}^*\chi_i^*}\right]\frac{1}{\mathcal{M}_A^*}, (33)$$

where $\alpha^* \equiv \alpha/(2.5 \times 10^{-6}~{\rm cm}^3~{\rm s}^{-1})$, $\zeta_{\rm CR}^* \equiv \zeta_{\rm CR}/(3 \times 10^{-17}~{\rm s}^{-1})$, and we have used equation (15). It follows that the molecular gas is typically very close to ionization equilibrium (although it is not necessarily close to chemical equilibrium). In simulations, the relevant comparison is between the flow time across a cell, $t_f/\mathcal{N}_g$, where $\mathcal{N}_g$ is the number of grid cells in the length of the box, and the ionization time. For our runs, which typically have $\mathcal{N}_g = 512$, we have $t_f/(\mathcal{N}_g t_{\rm ion,eq}) \simeq 6R_{AD}(\ell_0)$ for fiducial values of the parameters. Ionization equilibrium is thus a good approximation for all the cases we consider except $R_{AD}(\ell_0) = 0.12$.

To test our use of the approximation of ion conservation (see also the Appendix in Li et al. 2008), we ran several 256^3 models with time-dependent ionization for different values of R_{AD}. We find that the properties of the clumps in these runs are within a few percent of those in the corresponding 256^3 runs with ion conservation, with the exception of the ion density. In fact, the mean ion density in the entire box in the time-dependent case is less than that in the ion conservation case by up to a factor ~ 2. As a result, the value of the AD Reynolds number is reduced by a corresponding factor, as shown in Table 2. For large $R_{AD}(\ell_0)$, the gas is close to ionization equilibrium, so that $\bar{\rho}_i \propto \rho^{1/2}$. With this relation for the ion density, the mean ion density, and hence $R_{AD}(\ell_0)$, are reduced by only a small amount compared to the case of ion conservation for the low Mach number we are considering if the density PDF is a lognormal with a width similar to that found by Padoan & Nordlund (2002). For small $R_{AD}(\ell_0)$ the deviations from ionization equilibrium are larger, and correspondingly the difference between the time-dependent and ion conservation results are larger as well. In this paper, however, we are exploring the effects of changing $R_{AD}(\ell_0)$ by orders of magnitude, so changes of $\lesssim 2$ do not affect our conclusions.

4. PHYSICAL PROPERTIES OF CLUMPS

The formation of high-density clumps is a natural outcome in simulations of highly supersonic turbulence, whether a magnetic field is included or not. Furthermore, high-resolution turbulence simulations (e.g. Li et al. 2004; Padoan et al. 2007) produce a mass spectrum of clumps that qualitatively resembles the stellar initial mass function (IMF), with a peak at low mass and a power-law tail at high masses. Recent observations of molecular cores (e.g. Tachihara et al. 2002; Onishi et al. 2002; Alves, Lombardi, & Lada 2007) suggest a similarity between the stellar IMF and the core mass function. (We follow the terminology of Williams, Blitz, & McKee 2000 and use the term "core" to refer to the subset of clumps that are gravitationally bound and will form a star or small multiple stellar system.) Padoan & Nordlund (2002) and Padoan et al. (2007) have proposed a turbulent fragmentation theory for the IMF that relates the index of the velocity power spectrum to the slope of the higher-mass end of the clump mass spectrum. LMKF showed that ambipolar diffusion changes the velocity power index, and we confirm that conclusion in Paper III. If the turbulent fragmentation theory is correct, we would expect a change in the slope of the higher-mass end of the clump mass distribution between the ideal MHD and the AD turbulence simulations as well. (It should be noted that the Hennebelle & Chabrier 2008 theory leads to a much smaller predicted difference in the slope of the IMF in these two cases.)

We use a CLUMPFIND algorithm, based on the algorithm developed by Williams, De Geus, & Blitz (1994), to determine the clumps in our simulations. We define "clumps" as connected regions with a density larger than the mean density of the turbulent box and will use the term "ClMF" for "clump mass function," reserving "CMF" for "core mass function." This distinction is appropriate for our simulations since they do not include self gravity. The density contours are separated by $\delta\rho = 0.04\rho$, which Padoan et al. (2007) found to work well in distinguishing distinct clumps. In order to infer the effects of AD on the ClMF, we require the clumps

to be resolved. As mentioned in LMK, ZEUS-MPAD needs at least 3 to 6 zones to accurately distinguish the effects of AD from those of numerical diffusion. Therefore, we require clumps to have at least 6 zones in the mean radius, unless otherwise specified; this requirement is validated in the resolution study of ClMF in §5.2.1. In implementing this resolution requirement, we define the effective radius as $r_c \equiv (3V_c/4\pi)^{1/3}$, where V_c is the volume of the clump is determined by summing the volumes of each cell in the clump that has a density above threshold; thus, for a porous clump, r_c is less than the projected radius of the clump (see §4.3.2). This approach to setting the resolution requirement eliminates small, very porous clumps, which have a lot of structure that is not well resolved. By varying $\delta\rho$, we found that the number of clumps with mean radius larger than 6 cells does not change when the separation of the density contours is smaller than 4%, thereby justifying our choice of $\delta\rho$. Before constructing the ClMF, we verify that the clumps defined in our simulations satisfy the heavy-ion approximation.

4.1. The Heavy-Ion Approximation for Clumps

The condition for the validity of the heavy-ion approximation is $R_{\rm AD} \gg \mathcal{M}_{{\rm A}i}^2$, where the ion Alfvén Mach number, $\mathcal{M}_{{\rm A}i}$, is smaller than the total Alfvén Mach number, $\mathcal{M}_{\rm A}$, by a factor $(\rho_i/\rho)^{1/2} \ll 1$ (LMK). To calculate the AD Reynolds number of a clump, $R_{\rm AD, c}$, we use the 3D density-weighted velocity dispersion of the neutral gas, $\sqrt{3}\sigma_n$, inside a clump as the flow velocity and the mean diameter of the clump, $d_c = 2r_c$, as the length scale. The ion Alfvén Mach number of the clump, $\mathcal{M}_{{\rm A}i,c}$, is taken to be the rms value of $\mathcal{M}_{{\rm A}i}$ of all the cells in the clump. We can re-write the definition of $R_{\rm AD}$ in equation (6) for clumps as

$$R_{\rm AD, c}(D_c) \equiv \frac{4\pi\gamma_{\rm AD}\rho_i\rho_n D_c\sqrt{3}\sigma_n}{B_{\rm rms}^2} = \frac{\gamma_{\rm AD}\rho_n D_c\sigma_n}{\sqrt{3}\sigma_i^2}\mathcal{M}_{{\rm A}i,c}^2$$
$$\equiv C_{\rm HIA}\mathcal{M}_{{\rm A}i,c}^2. \qquad (34)$$

In Figure 1, we plot $\mathcal{M}_{{\rm A}i,c}^2$ versus $R_{\rm AD, c}$ for models m3c2r-1, m3c2r1, and m3c2r3 at $t = 3t_f$; the results for models m3c2r0 and m3c2r2 lie between the nearby models. The data points all have $R_{\rm AD, c} \gg \mathcal{M}_{{\rm A}i,c}^2$, even for model m3c2r-1, which has the smallest value of $R_{\rm AD}(\ell_0)$. We have verified that this is true at other times as well. LMKF found that the Heavy Ion Approximation was valid for a turbulent box provided $R_{\rm AD}(\ell_{vi})/\mathcal{M}_{{\rm A}i}^2 \gtrsim 30$, where ℓ_{vi} is the length scale for ion-velocity variations, which is generally significantly smaller than the size of the box. We do not know how ℓ_{vi} in the clumps compares with the clump diameters. If we assume that the two length scales are comparable, then the requirement for the validity of the Heavy Ion Approximation is $C_{\rm HIA} \gtrsim 30$. This is well satisfied for all the clumps except those in model m3c2r-1, which has $R_{\rm AD}(\ell) = 0.12$ and is the most diffusive run. For this run, the box as a whole has $C_{\rm HIA} \simeq 10$, and the Heavy Ion Approximation is at best marginally satisfied. We have not observed any problems associated with this, however.

Two interesting features of the results are worth noting. First, almost all the clumps have smaller values of $\mathcal{M}_{{\rm A}i}^2$ than the box as a whole; this is expected be-

cause of the linewidth-size relation. The few data points with slightly higher values of $\mathcal{M}_{{\rm A}i}^2$ are due to large statistical fluctuation in the ion density in a few clumps. Second, we note that the distribution of the data points is roughly parallel to the power law $R_{\rm AD} \propto \mathcal{M}_{{\rm A}i}^2$ (the straight line). This is because the factor $C_{\rm HIA}$ depends on two quantities, the column density, $\rho_n D_c$, and the velocity dispersion ratio, σ_n/σ_i^2, each of which is almost independent of $\mathcal{M}_{{\rm A}i}$.

4.2. Clump Mass Function (ClMF)

4.2.1. Resolution: The Sonic Length and the Inertial Range

In studying the properties of the clumps that arise in boxes with supersonic turbulence, two length scales are important: the sonic length, ℓ_s, and the minimum scale for the inertial range, $\ell_{\rm in, min}$, which corresponds to the wavenumber $k_{\rm in, max} = \ell_0/\ell_{\rm in, min}$. The sonic length, which is defined by the condition that the rms turbulent velocity in a box of size ℓ_s equal the sound speed, gives a characteristic scale for density fluctuations in a supersonically turbulent medium (Padoan 1995; Vázquez-Semadeni et al. 2003). The sonic length should be well resolved in numerical simulations since it is important to resolve these density fluctuations and the turbulent motions that produce them. The resolution condition is $\Delta x \ll \ell_s$, where Δx is the size of a grid cell; equivalently, in terms of the sonic wavenumber $k_s \equiv \ell_0/\ell_s$, we have $\ell_0/\Delta x \equiv \mathcal{N}_g \gg k_s$. We assume that the turbulence in the box exhibits a linewidth-size relation of the form[2]

$$\mathcal{M} = 3^{1/2}\frac{\sigma_{\rm nt}}{c_s} = \left(\frac{\ell_d}{\ell_s}\right)^q, \qquad (35)$$

where ℓ_d is the effective minimum driving scale; the corresponding wavenumber is $k_d \equiv \ell_0/\ell_d$. In our simulations, $k_d = 2$, and we find that the average Mach number in boxes of size ℓ_d is indeed very nearly equal to that for the entire box, $\mathcal{M} \simeq 3$. We also find $q \simeq \frac{1}{2}$ for $R_{\rm AD}(\ell_0)$ in the range 0.12-12; for $R_{\rm AD}(\ell_0) = 120$, 1200, we find $q \simeq \frac{1}{4}$. The sonic length in a simulation is then

$$\ell_s = \frac{\ell_0}{k_d\mathcal{M}^{1/q}}. \qquad (36)$$

Correspondingly, we have

$$k_s \equiv \frac{\ell_0}{\ell_s} = k_d\mathcal{M}^{1/q} \simeq 18 - 160, \qquad (37)$$

for $q = \frac{1}{2}$ and $q = \frac{1}{4}$, respectively. This satisfies the resolution condition $\mathcal{N}_g = 512 \gg k_s$ for $R_{\rm AD}(\ell_0) \leq 12$; for $R_{\rm AD}(\ell_0) = 120$, 1200, this resolution condition is only marginally satisfied.

Before leaving the topic of the sonic length, we note that it can be inferred for actual molecular clouds as well. For $q = \frac{1}{2}$ (the observed value–Heyer & Brunt 2004), the sonic length is related to the linewidth-size parameter

---

[2] Note that Krumholz & McKee (2005) defined the sonic length with respect to the 1D turbulent velocity, $\sigma_{\rm nt} = c_s(\ell_0/\ell_{s,\rm 1D})^q$, and adopted $q = \frac{1}{2}$; the two versions of the sonic length are related by $\ell_{s,\rm 1D} = 3^{1/(2q)}\ell_s$, corresponding to $\ell_{s,\rm 1D} = 3\ell_s$ for $q = \frac{1}{2}$.

σ_{pc} (eq. 53) by

$$\frac{\sigma_{\mathrm{pc}}^2}{1 \text{ pc}} = \frac{2c_s^2}{3\ell_s}, \qquad (38)$$

or

$$\ell_s = \frac{2c_s^2}{3\sigma_{\mathrm{pc}}^2} \text{ pc} = 0.0455 \left(\frac{T_1}{\sigma_{\mathrm{pc}}^{*\,2}}\right) \text{ pc.} \qquad (39)$$

We define the inertial range of the turbulence as the range of wavenumbers over which the power spectrum is a power law in k. In our simulations, this extends over the range $k_{\mathrm{in,\,max}} > k > 3$, where $k_{\mathrm{in,\,max}} \simeq 20$ for our 512^3 simulations and $\simeq 10$ for the 256^3 simulations reported in LMKF. For $k > k_{\mathrm{in,\,max}}$, numerical dissipation becomes increasingly important. Another way of expressing this condition is that with ZEUS, numerical dissipation becomes important at about 1/10th the minimum wavenumber, $k_{\mathrm{in,\,max}} \simeq 0.1 \times (\mathcal{N}_g/2)$. It is desirable to have the sonic length in the inertial range $k_s < k_{\mathrm{in,\,max}}$, and this is satisfied for the 512^3 simulations with $R_{\mathrm{AD}}(\ell_0) \leq 12$. Determining whether this condition is a general requirement for accurate simulations of supersonic turbulence is beyond the scope of this paper. We note that this condition becomes increasingly difficult to satisfy as the Mach number increases.

Figure 2 shows the clump mass distribution for the case of $R_{\mathrm{AD}}(\ell_0) = 1200$ (close to ideal MHD), at resolutions of 512^3 and 256^3. We can make an approximate relation between the clump masses and wavenumbers by associating a wavenumber $k_c \equiv \ell_0/D_c$, where D_c is the clump diameter, to each clump. The corresponding clump mass is approximately

$$\frac{M_c}{M_0} = \frac{4\pi}{3} \left(\frac{\bar{\rho}_c}{\bar{\rho}}\right) \frac{1}{(2k_c)^3}, \qquad (40)$$

where $\bar{\rho}_c$ is the average clump density. For the high-resolution run, the mean density of the clumps within the inertial range ($k_c < 20$) is $\bar{\rho}_c = 2.6\bar{\rho}$ (i.e., the mean density is 2.6 times the minimum clump density). The higher-mass part of the ClMF appears to be a power law (this is justified in §4.2.2 below). Observe that the slope of the ClMF changes at $\log M_c \sim -4.3$, corresponding to $k_c \simeq 30 = 1.5 k_{\mathrm{in,\,max}}$. In fact, the clumps with such a mass have $D_c \sim 12-20$ cells. This is similar to both the maximum wavenumber in the inertial range and to the sonic wavenumber, which are also shown in Figure 2, to within a factor of 2. In order to determine whether either of these parameters is associated with the change in slope, we also plot the clump mass spectrum for the corresponding 256^3 run, for which $k_{\mathrm{in,\,max}} = 10$ (vertical dashed line) is reduced by a factor 2 whereas k_s is unchanged. The results are clear: The break in the clump mass spectrum in the low-resolution run occurs at half the wavenumber as in the high-resolution one. Furthermore, there is no discernable effect associated with the sonic wavenumber, although it would be desirable to test this conjecture with both higher resolution simulations and for higher Mach numbers than $\mathcal{M} = 3$, the value in the present simulations. It therefore appears that the dominant effect in determining the deviation of the ClMF from a power law is the numerical dissipation that sets in for wavenumbers $k > k_{\mathrm{in,\,max}}$. The results

of our simulations can therefore address only the higher-mass portion of the ClMF, with a minimum diameter of 12 cells. Figure 3 shows the 3D spatial distribution of clumps, identified by CLUMPFIND with minimum diameter of 12 cells, from a snapshot of model m3c2r1.

4.2.2. *Implications for the Turbulent Fragmentation Model for the IMF*

As remarked above, the similarity between the core mass function and the stellar IMF suggests that the IMF may be defined during the formation of cores inside molecular clouds. In the turbulent fragmentation model of Padoan & Nordlund (2002) and Padoan et al. (2007), the mass distribution of cores (i.e., gravitationally unstable clumps) has the form

$$\frac{d\mathcal{N}_{\mathrm{core}}}{d\ln m} \propto \left[1 + \mathrm{erf}\left(\frac{4\ln m + \sigma_x^2}{2\sqrt{2}\sigma_x}\right)\right] m^{-\Gamma}, \qquad (41)$$

where σ_x is the dispersion of the density PDF. The power-law index of the core mass function at high masses, Γ, is related to the index, n_v, of the velocity power spectrum, $P(k)dk \propto k^{-n_v}dk$, by

$$\Gamma = \frac{3}{4 - n_v} \qquad (42)$$

for the strong-field, ideal MHD case ($B \geq B_{\mathrm{cr}}$), and

$$\Gamma = \frac{3}{5 - 2n_v} \qquad (43)$$

for the weak-field, ideal MHD case ($B < B_{\mathrm{cr}}$), which includes the hydrodynamic case (Padoan et al. 2007); here the critical magnetic field B_{cr} is defined by the condition that the postshock gas pressure be comparable to the postshock magnetic pressure. Hennebelle & Chabrier (2008) have introduced an improved theory for the IMF, but we cannot comment on the differences between their results and those of Padoan et al. (2007) since our simulations do not include self-gravity. As noted above, the Hennebelle & Chabrier theory predicts a much smaller difference in the slope of the IMF between the magnetic and non-magnetic cases than does the theory of Padoan et al.

The simulations of Padoan et al. (2007) do not include self-gravity. Based on the discussion at the beginning of §5 below, we note that if one specifies the temperature and adopts a linewidth-size relation, then it is possible to fix one parameter arbitrarily. For the Mach number they adopted ($\mathcal{M} = 10$), their box size of $\ell_0 = 6$ pc is in good agreement with the linewidth size relation in equation (53). However, they chose a density $\bar{n}_{\mathrm{H}} = 2 \times 10^4$ cm^{-3}, which results in a virial parameter $\alpha_{\mathrm{vir}} \simeq 0.028$, far lower than observed values.

In contrast to the Padoan et al simulations, we have included an additional physical process—ambipolar diffusion—so that the strength of the self-gravity is determined by the parameter governing that process, $R_{\mathrm{AD}}(\ell_0)$, as discussed in §2.4. For the value of $\mathcal{M}_{\mathrm{A}}$ we have adopted ($\mathcal{M}_{\mathrm{A}} = 0.67$) and for the fiducial values of the ion-neutral coupling coefficient γ_{AD} and the ionization parameter χ_i, the virial parameter of the box is $\alpha_{\mathrm{vir}} = 41/R_{\mathrm{AD}}(\ell_0)^2$ (eq. 30). This is unphysically low for $R_{\mathrm{AD}}(\ell_0) \gtrsim 6$: in nature, large values of the AD

Reynolds number are accompanied either by large values of $\mathcal{M}_A$ (which is unlikely according to the results of Crutcher 1999) or by larger ionizations than implied by $\chi_i^* = 1$. The core Bonnor-Ebert mass—that is, the Bonnor-Ebert mass based on the turbulent pressure in the ambient medium (eq. A50)—in our simulations is

$$M_{\text{BE, core}} = \frac{\sqrt{3}}{\mathcal{M}} M_{\text{BE}} = 0.84 \frac{\alpha_{\text{vir}}^{1/2} T_1^2}{\sigma_{\text{pc}}^{*}{}^2} \ M_\odot$$
$$\rightarrow \frac{5.4}{R_{\text{AD}}(\ell_0)} \ M_\odot, \tag{44}$$

where the last expression is for fiducial values of the parameters. Of the five AD models in Table 2, only model m3c2r1, with $R_{\text{AD}}(\ell_0) = 12$ (comparable to the observed values), yields a physically plausible Bonnor-Ebert mass. We therefore do not attempt to put our clump mass function in physical units here (physical units are discussed in §5 below). What we can study is the slope of the higher-mass portion of the ClMF, which is independent of the choice of units.

Ambipolar diffusion could introduce two changes in the value of Γ: First, the relation between Γ and n_v could be different, varying from the hydrodynamic relation to the MHD one as $R_{\text{AD}}(\ell_0)$ goes from 0 to ∞. Second, as shown in LMKF, the value of n_v also depends on $R_{\text{AD}}(\ell_0)$. In the pure hydrodynamic case, $n_v = 2$ for supersonic turbulence, whereas in the MHD case the value of n_v is not precisely known and could depend on the plasma β.

In Figure 4, we show the ClMFs of models m3c2r-1, m3c2r1, and m3i. LMKF showed that the density correlation between data sets at different times approaches zero in a time slightly less than t_f. Therefore, in order to build up the statistics, we use three data sets in each model run, at $t \simeq t_f$, $2t_f$ and $3t_f$. Adding all the clumps together to form a single data set, we use reduced χ^2 fitting to determine the higher-mass slope of the core mass function, Γ_{fit}. We face two problems in determining Γ_{fit}: First, we do not know the the range of masses to include in the "higher-mass" data, and second, we do not want our answer to depend on the size of the bins used in binning the data. We begin by dividing the data into 20 logarithmically spaced mass bins. To address the first problem, we carry out fits beginning with only the three highest-mass bins, and then steadily increase the number of bins used in the fitting until the peak of ClMF is reached. Initially, the value of χ^2 drops as the number of bins increases, since more data are contributing to the determination of the slope. However, when the number of bins is large enough that the ClMF begins to deviate from a power law, the reduced χ^2 will increase. To address the second problem, we increase the number of bins from 20 to 40 in increments of 5 and adopt the value of Γ_{fit} with the smallest reduced χ^2 from all five sets of fitting. Usually, the slopes corresponding to the minimum reduced χ^2 from different total bin numbers are close to each other. The resulting slopes are listed in Table 3.

In view of the noise fluctuations in the higher-mass range of the ClMF, we have performed a two-sample Kolmogorov-Smirnov (K-S) test to determine whether this part of the ClMF can be fit with a power law. The mass range extends from the highest mass bin to the breakpoint determined by the χ^2 fitting procedure described above. The null hypothesis is that the higher-mass end of the ClMF from the simulation has the same distribution as a power law. Our results show that the K-S test on all five AD models and the ideal MHD model fails to reject the null hypothesis at the 5% confidence level. The p-values of all the K-S tests with different binning are between 0.49 and 0.97. We conclude that the higher-mass portion of the ClMF is statistically consistent with a power law. For the ideal mhd case (model m3i) and for $R_{\text{AD}}(\ell_0) = 12$ (model m3c2r1), the power law extends over the entire inertial range. However, in the limit of low $R_{\text{AD}}(\ell_0)$ (model m3c2r-1), the power law extends only over the upper half of the inertial range; higher resolution and/or more samples are needed to determine if the inertial range is consistent with a power law in this case.

With these 512^3 models, the clump statistics are adequate to demonstrate that the higher-mass slopes depend on R_{AD}. If turbulent fragmentation is correct, this is no surprise because LMKF found that the spectral indexes of the velocity power spectra also depend on R_{AD}. Here we draw on the results of Paper III, which gives more accurate values of the spectral index for the velocity of the neutrals, $n_{vn}(k)$, than LMKF (see Table 3). The trend of spectral index changing from an Iroshnikov-Kraichnan (Iroshnikov 1963; Kraichnan 1965) to Burgers spectrum (Burgers 1974) as one goes from large to small R_{AD} is still clear, as reported in LMKF.

In the limit of ideal MHD (model m3i), the higher-mass slope is $\Gamma_{\text{fit}} = 1.21 \pm 0.09$ (see Figure 3), which agrees quite well with the prediction $\Gamma = 1.18$ from equation (42) with spectral index $n_v = 1.45 \pm 0.05$. Note that Padoan et al. (2007) get somewhat different results ($n_v = 1.9$ and $\Gamma = 1.4$), but this is presumably due to the difference in flow conditions: they have $\mathcal{M} = 10$ and $\beta = 1$, whereas we have $\mathcal{M} = 3$ and $\beta = 0.1$. In their hydrodynamic simulations, Ballesteros-Paredes et al. (2006) found that the shape of the ClMF depends on the Mach number of the turbulence, consistent with our result. If the shape of the ClMF is significantly affected by the flow conditions, then the Padoan et al. (2007) model would imply that the IMF depends on the environment, since regions of star formation do not all have similar physical conditions. As Ballesteros-Paredes et al. (2006) point out, this could be problematic in view of observational support for an IMF that is approximately universal.

For the model m3c2r1, which has $R_{\text{AD}} = 12$, comparable to the observed value (§2.3), the higher-mass slope is $\Gamma_{\text{fit}} = 1.43 \pm 0.10$, which is consistent with the Salpeter value. As noted above, in the limit of low R_{AD} (model m3c2r-1), we are unable to fit the data with a power law that extends over the entire inertial range; The slope for the high-mass portion of the range for which a fit is possible is $\Gamma_{\text{fit}} = 2.41 \pm 0.14$, which continues the trend that the slope increases as $R_{\text{AD}}(\ell_0)$ decreases. Since this slope applies to only part of the inertial range, however, we are unable to check the validity of equation (43), which relates the slope of the ClMF to the velocity power spectrum in the weak field case. Consistent with the results of Padoan et al. (2007), this slope is significantly greater than the Salpeter value of the higher-mass slope, $\Gamma = 1.35$.

Comparison of numerical simulations of turbu-

lence with either pure hydrodynamics or ideal MHD has shown that magnetic fields suppress fragmentation (e.g. Passot, Vázquez-Semadeni, & Pouquet 1995; Gammie et al. 2003; Padoan et al. 2007; Hennebelle & Teyssier 2008). We can see this effect in our simulations by comparing the ClMFs of models m3c2r-1, in which the neutrals are almost purely hydrodynamic, and m3i, with ideal MHD. Figure 4 shows that the number of clumps in the low-R_{AD} models is greater than in the high-R_{AD} models, except at the higher-mass end: The total number of clumps with $D_c > 12$ cells from the three time snapshots in the quasi-hydrodynamic model m3c2r-1 is 2093 (Table 3), whereas it is 1033 in model m3i. The total mass of clumps in model m3c2r-1 is $\sim 0.106 M_0$, whereas it is $\sim 0.092 M_0$ in model m3i. On average, the mass per clump in the quasi-hydrodynamic model m3c2r-1 is smaller than that in the ideal MHD model, which is also consistent with prior simulations.

The turbulent fragmentation model for the IMF predicts that the core mass function (CMF) (i.e., the mass function of gravitationally bound clumps) is the same as the clump mass function (ClMF) at high masses, and it is based on the assumption that the IMF is proportional to the core mass function (the latter is predicted in the work of Matzner & McKee 2000). Padoan et al. (2007) emphasize that the predicted ClMF for hydrodynamic turbulence is much steeper than for ideal MHD turbulence, and our work confirms this. Our work shows that there is a continuous variation in the higher-mass slope of the ClMF due to the effects of ambipolar diffusion, such that the fraction of stars born at high mass should increase with R_{AD}.

4.3. Mass-To-Flux Ratios

Ambipolar diffusion plays an important role in the core collapse process when the clump mass is less than or comparable to the magnetic critical mass (eq. 26). Observationally, only a limited number of cores have measured mass-to-flux ratios due to the difficulty in making precise Zeeman measurements. Furthermore, observations give only the line-of-sight values for the magnetic field and column density, so the value of $\mu_\Phi \propto M/\Phi$ for any particular core is necessarily uncertain. From a study of 34 dark cloud cores, Troland & Crutcher (2008) found an average value of $\mu_{\Phi,c} = 1.4 - 2.1$ after allowance for projection effects; the smaller value is based on flattened clouds, whereas the larger one is for spherical ones. The median values are larger by about 20%. Observed cores are thus somewhat magnetically supercritical.

4.3.1. Resolution Study

In this section, we check the convergence of the mass-to-flux ratios of the clumps by comparing the results from the 256^3 and 512^3 runs for model m3c2r3. To carry out the resolution study, we consider only clumps that have a mass at least equal to the minimum mass of clumps with $r_c \geq 12$ cells in the 512^3 model; for the 256^3 run, this corresponds to $r_c \gtrsim 6$ cells. For easy comparison of clump mass-to-flux ratios among models, we eliminate the dependence of the mass-to-flux ratio on clump mass by plotting the ratio $(\mu_{\Phi,c}/\mu_{\Phi,0})/(M_c/M_0)^{1/3}$ versus M_c/M_0 for both the 256^3 and 512^3 runs in Figure

5. Curve fitting shows that the slope of the 256^3 data is 0.06 ± 0.03 and the slope of 512^3 data is 0.07 ± 0.02. The mean values of $(\mu_{\Phi,c}/\mu_{\Phi,0})/(M_c/M_0)^{1/3}$ are 1.68 ± 0.03 and 1.78 ± 0.03 for the 256^3 and 512^3 models, respectively. We conclude that the mass-to-flux ratios of clumps in the 512^3 model are converged.

4.3.2. Effect of $R_{\mathrm{AD}}(\ell_0)$ on the Mass-to-Flux Ratio

As discussed in §4.2.2 above, our choice of parameters allows us to study the effect of varying $R_{\mathrm{AD}}(\ell_0)$ on the mass-to-flux ratios, but at the expense of considering models that would be unphysical were gravity to be included: Equation (31) implies $\mu_{\Phi,0} = 0.17 R_{\mathrm{AD}}(\ell_0)/(\gamma_{\mathrm{AD}}{}^*\chi_i^*)$ for our simulations, which is in the observed range only for the $R_{\mathrm{AD}}(\ell_0) = 12$ case. What is of interest then is how the normalized values of the mass-to-flux ratio vary with R_{AD}. For example, the ratio of the mass-to-flux ratio for an individual clump, $\mu_{\Phi,c}$, to that for the entire box is

$$\frac{\mu_{\Phi,c}}{\mu_{\Phi,0}} = \frac{M_c}{B_c \pi R_{c,\perp}^2} \cdot \frac{B_0 \ell_0^2}{M_0} = \left(\frac{B_0}{B_c}\right)\frac{\Sigma_c}{\Sigma_0} \simeq \frac{\Sigma_c}{\Sigma_0}, \quad (45)$$

where $R_{c,\perp}$ is the radius of the clump normal to the field threading the clump, B_c, and Σ_0 is the mean surface density for the turbulent box. For the cases we consider, the mean field in the clump is close to the mean field of the whole box since the relatively small value of the Alfvén Mach number, $\mathcal{M}_{\mathrm{A}} = 0.67$, leads to a relatively uniform field, as discussed in §4.4 below. As a result, for most clumps the mass-to-flux ratios are just proportional to the surface densities. The ratio Σ_0/Σ_c is just the number of clumps along a flux tube. Furthermore, since the density of the clumps is typically a few times the threshold density (see below eq. 40) and is thus approximately constant, it follows that the mass-to-flux ratio in the clumps is proportional to the cube root of the clump mass:

$$\mu_{\phi,,c} \propto \Sigma_c \propto \rho_c R_c \propto R_c \propto M_c^{1/3}. \quad (46)$$

We now use our simulations to determine whether ambipolar diffusion in a turbulent medium affects the mass-to-flux ratio in clumps, even in the absence of self-gravity. In order to ensure that the clumps we study are in the higher-mass, power-law regime of the clump mass distribution so that numerical effects are minimal, we choose a minimum clump mass that is above the threshold for the higher-mass regime in all cases. This minimum mass corresponds to a minimum clump radius of $r_c = 6$ cells.

To determine how ambipolar diffusion affects the mass-to-flux ratio, we compute the value of $(\mu_{\Phi,c}/\mu_{\Phi,0})/(M_c/M_0)^{1/3}$ for all clumps in each model and plot the results in Figure 6. The mean values of $\mu_{\Phi,c}/\mu_{\Phi,0}$ for the three models are also tabulated in Table 3 and are shown as the horizontal lines in Figure 6. In all the models, the values of $\mu_{\Phi,c}$ for the clumps are smaller than $\mu_{\Phi,0}$ for the whole box due to fragmentation along flux tubes. This effect has been observed in other MHD turbulence simulations (Vázquez-Semadeni et al. 2005a; Tilley & Pudritz 2007). The typical value of the normalized mass-to-flux ratio, $\mu_{\Phi,c}/\mu_{\Phi,0} \sim 0.1$, is set by our resolution, since the number of clumps increases with decreasing size and $\mu_{\Phi,c}$ scales as $M_c^{1/3}$. We observe from Figure 6 and Table 3 that $\langle\mu_{\Phi,c}\rangle/\mu_{\Phi,0}$

shows a small systematic increase from the large R_{AD} model to the small and moderate R_{AD} models.

This table also shows that the mean density of clumps, $\langle \rho_c \rangle$, in the three models increases systematically as R_{AD} decreases. The dispersion in the values of $\mu_{\Phi,c}/\mu_{\Phi,0}/(M_c/M_0)^{1/3}$ in Figure 6 shows a significant variation as R_{AD} decreases. The dispersions of mass-to-flux ratio (not mass-to-flux divided by $M^{1/3}$) are given in Table 3. The dispersion for $R_{\mathrm{AD}}(\ell_0) = 12$ is almost twice that for $R_{\mathrm{AD}}(\ell_0) = 1200$. The larger dispersion of $\mu_{\Phi,c}$ and higher density of clumps at $R_{\mathrm{AD}}(\ell_0) = 12$ than at high $R_{\mathrm{AD}}(\ell_0)$ suggest that material can more easily cross magnetic field lines as R_{AD} decreases. A further decrease in $R_{\mathrm{AD}}(\ell_0)$ to 0.12 results in a higher density, but increased fragmentation of the clumps reduces the dispersion somewhat. We conclude that, even in the absence of self-gravity, ambipolar diffusion has an effect on the mass-to-flux ratios of clumps.

4.4. *Other Physical Properties of Clumps*

In this section, we summarize a number of other physical properties of the clumps as functions of $R_{\mathrm{AD,c}}$ in Figure 7 by comparing the two models m3c2r-1 [$R_{\mathrm{AD}}(\ell_0) = 0.12$, strong AD] and m3c2r3 [$R_{\mathrm{AD}}(\ell_0) = 1200$, strong ion-neutral coupling], which represent the two extremes of ion-neutral coupling among our simulations. Figure 7 gives side-by-side plots of the normalized clump radii, r_c/ℓ_0, the ion and neutral densities, $\rho_{i,c}/\rho_0$ and $\rho_{n,c}/\rho_0$, magnetic energy density, $U_{B,c}/U_{B,0}$, clump mass, M_c/M_0, and ionization mass fraction, χ_i, for clumps for the two models.

Figure 7a shows that the normalized radii of the clumps in the strong-coupling model (m3c2r3) are, on average, larger than those for the strong AD model (m3c2r-1). This is a result of more fragmentation in the strong AD case. The largest radius in m3c2r3 is about double that in m3c2r-1. Since we require clumps to have a radius larger than 6 cells, there is a sharp truncation in the size distributions at $r_c/\ell_0 = 6/512 = 0.012$. Vázquez-Semadeni et al. (2005b) found that clumps in the non-magnetic case were smaller than those in the ideal MHD case, consistent with our result.

Note that the clumps in model m3c2r3 have a smaller range of $R_{\mathrm{AD,c}}$ because of the strong coupling between ions and neutrals. This is seen in all other properties as well. Figures 7b and 7c show the normalized mean ion and neutral densities of the clumps. The sharp bottom edge in Figures 7a and 7c is the result of the density threshold $\rho_c \geq \rho_0$ we chose in defining the clumps. The variations in ion density are much smaller in the strong coupling case than in the strong AD case. This is also reflected in the ionization mass fraction in Figure 7f. The ionization mass fraction of clumps in the strong coupling model is about constant, but that of clumps in the strong AD model varies by almost 3 orders of magnitude. In Figure 7d, the magnetic field is barely perturbed by the turbulence in model m3c2r-1 because of weak coupling; the magnetic field energy density in the clumps, $U_{B,c}$, is very nearly the same as that for the whole box. Although the magnetic field is perturbed more in model m3c2r3, most clumps have $U_{B,c}$ within 50% of that in the box. Figure 7e shows that the largest clumps in m3c2r3 are more massive than the largest ones in m3c2r-1. This

larger mass is due to a larger size, since the densities in the two models are about the same, and can be understood as the result of magnetic suppression of fragmentation, as discussed in §5.2.2. The clump properties shown in Figure 7 include clumps down to $r_c = 6$ cells. From this figure, we see that the global physical properties of clumps scale smoothly from $r_c = 6$ cells to the largest clump.

5. PHYSICAL UNITS FOR SIMULATIONS OF TURBULENT BOXES WITH AMBIPOLAR DIFFUSION

The results of our simulations have been reported in dimensionless form. How can they be converted to physical values? A simulation of an isothermal, magnetized, turbulent box is characterized by three dimensional parameters—the size of the box, ℓ_0, the mean density in the box, $\bar{n}_{\mathrm{H}}$, and the isothermal sound speed, c_s—and two dimensionless ones—the 3D sonic Mach number, $\mathcal{M} = 3^{1/2}\sigma_{\mathrm{nt}}/c_s$ and the plasma-β parameter, $\beta \equiv 8\pi\bar{\rho}c_s^2/B_{\mathrm{rms}}^2$ (Ostriker, Gammie, & Stone 1999; Padoan & Nordlund 1999). Here $\bar{n}_{\mathrm{H}}$ is the mean density of hydrogen nuclei, σ_{nt} is the 1D nonthermal velocity dispersion and $B_{\mathrm{rms}} \equiv \langle B^2 \rangle^{1/2}$ is the rms magnetic field. In the absence of other physical processes, all these parameters can be selected arbitrarily, although the value of $c_s \propto T^{1/2}$ is tightly constrained for molecular clouds, which generally have temperatures in the range $10-20\,\mathrm{K}$.

Inclusion of a new physical process, such as ambipolar diffusion, introduces a new dimensional constant, in this case the ion-neutral coupling parameter, γ_{AD}. Correspondingly, a new dimensionless parameter (in this case, R_{AD}) can be formed and the number of independent dimensional parameters is reduced by one. For a given sound speed, there is thus one independent dimensional parameter, such as the density, in simulations of ambipolar diffusion; such simulations are therefore scale free. Treatments of ambipolar diffusion require specification of the ionization, which in principle can introduce another dimensionless parameter that in turn would determine the scale. However, as discussed in §A.3, the Heavy Ion Approximation eliminates this constraint.

Adoption of a linewidth-size relation, as is observed in molecular clouds (Larson 1981), also reduces the number of independent dimensional parameters by one. Hence, if an isothermal system satisfies a linewidth-size relation and is subject to ambipolar diffusion, then its velocity scale is set by the isothermal sound speed, $c_s \propto T^{1/2}$, and its size and mean density are determined by dimensionless parameters. In this case, a given simulation applies to only one set of parameters describing the box. This is discussed further in the Appendix, which gives explicit expressions for properties of turbulent boxes in the general case, when they satisfy a linewidth-size relation, and for self-gravitating boxes. Here we present the scaling for our simulations of turbulent boxes with ambipolar diffusion.

5.1. *General Scaling Relations*

To determine how simulations of a turbulent box with ambipolar diffusion can be scaled to physical systems, we use equation (15) to solve for the size of the simulation box, ℓ_0. We find that it is determined by the remaining two dimensional parameters ($\bar{n}_{\mathrm{H}}$ and T) along with five

dimensionless parameters $[R_{\mathrm{AD}}(\ell_0), \gamma_{\mathrm{AD}}{}^*, \chi_i^*, \beta$ and $\mathcal{M}]$:

$$\ell_0 = 0.031 \left[\frac{R_{\mathrm{AD}}(\ell_0)}{\gamma_{\mathrm{AD}}{}^* \chi_i^*} \right] \frac{\mathcal{M}}{\mathcal{M}_{\mathrm{A}}{}^2} \left(\frac{T_1}{\bar{n}_{\mathrm{H},3}} \right)^{1/2} \quad \mathrm{pc}, \qquad (47)$$

The flow time across the box, the mass in the box, and the column density are then

$$t_f = \frac{\ell_0}{\mathcal{M}c_s} = 1.62 \times 10^5 \left[\frac{R_{\mathrm{AD}}(\ell_0)}{\gamma_{\mathrm{AD}}{}^* \chi_i^*} \right] \frac{1}{\mathcal{M}_{\mathrm{A}}{}^2 \bar{n}_{\mathrm{H},3}^{1/2}} \quad \mathrm{yr}, \qquad (48)$$

$$M_0 = \bar{\rho} \ell_0^3 = 1.06 \times 10^{-3} \left[\frac{R_{\mathrm{AD}}(\ell_0)}{\gamma_{\mathrm{AD}}{}^* \chi_i^*} \right]^3 \frac{\mathcal{M}^3 T_1^{3/2}}{\mathcal{M}_{\mathrm{A}}{}^6 \bar{n}_{\mathrm{H},3}^{1/2}} \quad M_\odot, \qquad (49)$$

$$N_{\mathrm{H}} = \bar{n}_{\mathrm{H}} \ell_0 = 9.6 \times 10^{19} \left[\frac{R_{\mathrm{AD}}(\ell_0)}{\gamma_{\mathrm{AD}}{}^* \chi_i^*} \right] \frac{\mathcal{M}}{\mathcal{M}_{\mathrm{A}}{}^2} (\bar{n}_{\mathrm{H},3} T_1)^{1/2} \quad \mathrm{cm}^{-2} \quad (50)$$

Note that these scalings are preserved by the Heavy-Ion Approximation, in which the ion mass fraction ($\propto \chi_i^*$) is increased and the ion-neutral coupling coefficient ($\propto \gamma_{\mathrm{AD}}{}^*$) is decreased by the same factor. The strength of the magnetic field does not depend on $R_{\mathrm{AD}}(\ell_0)$,

$$B = (4\pi \rho c_s^2)^{1/2} \frac{\mathcal{M}}{\mathcal{M}_{\mathrm{A}}} = 3.2 (\bar{n}_{\mathrm{H},3} T_1)^{1/2} \frac{\mathcal{M}}{\mathcal{M}_{\mathrm{A}}} \quad \mu\mathrm{G}. \quad (51)$$

As discussed in §2.4, simulations of gas in which the ionization scales as $n_{\mathrm{H}}^{-1/2}$ have an implicit value of the virial parameter, α_{vir}, given by equation (30). Actual physical systems have $\alpha_{\mathrm{vir}} \gtrsim 1$, since violations of this inequality lead to gravitational motions that raise α_{vir} up to order unity. Hence, this sets a lower limit on the product of the ionization parameter and the AD coupling parameter for a given value of $R_{\mathrm{AD}}(\ell_0)$,

$$\gamma_{\mathrm{AD}}{}^* \chi_i^* \gtrsim \frac{R_{\mathrm{AD}}(\ell_0)}{14.2 \mathcal{M}_{\mathrm{A}}{}^2}. \qquad (52)$$

The lower limit on the ionization corresponds to the case of gravitationally bound clouds and clumps discussed in §2.4 (for spherical clouds, the coefficient 14.2 is replaced by $14.2/c_V^{1/2} \simeq 19.7$).

5.2. *Scaling with the Linewidth-Size Relation*

Most molecular gas in the Galaxy is observed to obey a linewidth-size relation

$$\sigma_{\mathrm{nt}} = \sigma_{\mathrm{pc}} R_{\mathrm{pc}}^{1/2}, \qquad (53)$$

where R_{pc} is the radius of the region measured in pc and typically $\sigma_{\mathrm{pc}} \simeq 0.72$ km s^{-1} (McKee & Ostriker 2007). The linewidth-size relation is quite general: it applies to within a factor ~ 3 to molecular gas ranging from small clumps much less than 1 pc in size to GMCs (Falgarone et al. 2009). Taking $R = \ell_0/2$ and noting that $\mathcal{M}$ is the 3D Mach number, we find

$$\mathcal{M} = 3^{1/2} \frac{\sigma_{\mathrm{nt}}}{c_s} = \left(\frac{3\ell_0}{2c_s^2} \right)^{1/2} \frac{\sigma_{\mathrm{pc}}}{(1 \mathrm{\ pc})^{1/2}} = 4.69 \frac{\sigma_{\mathrm{pc}}^* \ell_{0,\mathrm{pc}}^{1/2}}{T_1^{1/2}}, \qquad (54)$$

where

$$\sigma_{\mathrm{pc}}^* \equiv \frac{\sigma_{\mathrm{pc}}}{0.72 \mathrm{\ km\ s}^{-1}}. \qquad (55)$$

Falgarone & McKee (2010) have shown that this *turbulence-dominated linewidth-size relation* applies only

when

$$N_{\mathrm{H}} < N_{\mathrm{LWS}} = 1.3 \times 10^{22} \sigma_{\mathrm{pc}}^{*\,2} \quad \mathrm{cm}^{-2}, \qquad (56)$$

or, equivalently, when

$$\bar{n}_{\mathrm{H}} < \bar{n}_{\mathrm{LWS}} = 9.6 \times 10^4 \left(\frac{\sigma_{\mathrm{pc}}^{*\,4}}{\mathcal{M}^2 T_1} \right). \qquad (57)$$

For larger values of the column density and density, the linewidth-size relation must take the effects of self-gravity into account. The resulting *virialized linewidth-size relation* has $\sigma \propto (\Sigma \ell)^{1/2}$ and is equivalent to setting the virial parameter equal to unity, $\alpha_{\mathrm{vir}} = 1$ (Heyer et al. 2009; see §A.2.1). The linewidth is greater than that in the turbulence-dominated case due to the effects of self gravity.

When the turbulence-dominated linewidth-size relation applies, so that N_{H} and $\bar{n}_{\mathrm{H}}$ satisfy the inequalities in equations (56) and (57), then the size of the simulation box is determined by equation (54):

$$\ell_0 = 0.0454 \left(\frac{\mathcal{M}^2 T_1}{\sigma_{\mathrm{pc}}^{*\,2}} \right) \quad \mathrm{pc}. \qquad (58)$$

With the aid of equation (47), one can then express the density in terms of the linewidth-size parameter, σ_{pc}^*,

$$\bar{n}_{\mathrm{H}} = 9.6 \times 10^4 \left(\frac{\sigma_{\mathrm{pc}}^{*\,4}}{\mathcal{M}^2 T_1} \right) \left[\frac{R_{\mathrm{AD}}(\ell_0)}{14.2 \mathcal{M}_{\mathrm{A}}{}^2 \gamma_{\mathrm{AD}}{}^* \chi_i^*} \right]^2 \quad \mathrm{cm}^{-3} \quad (59)$$

$$= \bar{n}_{\mathrm{LWS}} \left[\frac{R_{\mathrm{AD}}(\ell_0)}{14.2 \mathcal{M}_{\mathrm{A}}{}^2 \gamma_{\mathrm{AD}}{}^* \chi_i^*} \right]^2, \qquad (60)$$

where the factor in brackets is $\lesssim 1$ since the corresponding virial parameter must be $\gtrsim 1$ (eq. 52). Similarly, one can show that

$$N_{\mathrm{H}} = N_{\mathrm{LWS}} \left[\frac{R_{\mathrm{AD}}(\ell_0)}{14.2 \mathcal{M}_{\mathrm{A}}{}^2 \gamma_{\mathrm{AD}}{}^* \chi_i^*} \right]^2 \qquad (61)$$

with the aid of equation (56). The mass corresponding to N_{LWS} and $\bar{n}_{\mathrm{LWS}}$—i.e., the maximum mass at which the turbulence-dominated linewidth size relation holds—is M_{LWS}, which is given in equation (A41). The mass in the simulation box is given in terms of M_{LWS} by

$$M_0 = M_{\mathrm{LWS}} \left[\frac{R_{\mathrm{AD}}(\ell_0)}{14.2 \mathcal{M}_{\mathrm{A}}{}^2 \gamma_{\mathrm{AD}}{}^* \chi_i^*} \right]^2. \qquad (62)$$

On the other hand, when the system being simulated is self-gravitating, then $\alpha_{\mathrm{vir}} \sim 1$ and the inequality in equation (52) is replaced by an equality. Equations (47), (49), and (50) show that in this case, $\ell_0 \propto \bar{n}_{\mathrm{H}}^{-1/2}$ and $M_0 \propto \bar{n}_{\mathrm{H}}^{-1/2}$ are smaller than in the turbulence-dominated case, whereas $N_{\mathrm{H}} \propto \bar{n}_{\mathrm{H}}^{1/2}$ is larger. The general case is discussed in the Appendix, §A.2.3.

5.3. *Physical Parameters for Simulations*

We are now in a position to discuss the physical parameters corresponding to our simulations. For simplicity, we shall assume that the temperature is $T = 10$ K and that the linewidth-size parameter has its fiducial value,

$\sigma_{\mathrm{pc}}^* = 1$, corresponding to $\sigma_{\mathrm{pc}} = 0.72$ km s^{-1}. The maximum column density for the turbulence-dominated linewidth-size relation is $N_{\mathrm{LWS}} = 1.3 \times 10^{22}$ cm^{-2}, and since the Mach number is $\mathcal{M} = 3$, the corresponding maximum density is $n_{\mathrm{LWS}} = 1.1 \times 10^4$ cm^{-3}. We shall focus on the four cases $R_{\mathrm{AD}}(\ell_0) = 1.2, 12, 120, 1200$, since the $R_{\mathrm{AD}}(\ell_0) = 0.12$ case was done to model the transition to the hydrodynamic limit. Recall that the clouds in Crutcher (1999)'s observations have a logarithmic mean value $\langle R_{\mathrm{AD}} \rangle_{\mathrm{log}} = 17$, comparable to the value in the $R_{\mathrm{AD}}(\ell_0) = 12$ simulation. The $R_{\mathrm{AD}}(\ell_0) = 1.2$ simulation has a somewhat smaller value of R_{AD}, and the $R_{\mathrm{AD}}(\ell_0) = 120$ simulation a somewhat larger value, than any of the clouds in that sample; however, it must be borne in mind that this sample by no means covers all the types of molecular gas in the Galaxy. In particular, the $R_{\mathrm{AD}}(\ell_0) = 1200$ run is relevant to the outer parts of GMCs, where the ionization is dominated by C$^+$.

The virial parameter associated with a given value of $R_{\mathrm{AD}}(\ell_0)$ in our simulations is

$$\alpha_{\mathrm{vir}} = \left[\frac{R_{\mathrm{AD}}(\ell_0)}{6.4 \gamma_{\mathrm{AD}}^* \chi_i^*} \right]^{-2} \qquad (63)$$

from equation (30). Since our simulations have $\mathcal{M}_A = 0.67$, the constraint on the ionization set by the requirement $\alpha_{\mathrm{vir}} \gtrsim 1$ implies (eq. 52)

$$R_{\mathrm{AD}}(\ell_0) \lesssim 6.4 \gamma_{\mathrm{AD}}^* \chi_i^*. \qquad (64)$$

First consider the case in which $R_{\mathrm{AD}}(\ell_0) = 1.2$. We assume that the ionization and coupling parameters have their fiducial values ($\gamma_{\mathrm{AD}}^* = \chi_i^* = 1$); the ionization constraint is then well satisfied. The virial parameter is $\alpha_{\mathrm{vir}} = 28$ from equation (63), so the self-gravity is negligible in the system being simulated. Equations (47), (49), (50) and (51) imply that the size of the system is $\ell_0 = 0.25 \bar{n}_{\mathrm{H},3}^{-1/2}$ pc, the mass is $M = 0.54 \bar{n}_{\mathrm{H},3}^{-1/2} M_\odot$, the column density is $N_{\mathrm{H}} = 7.7 \times 10^{20} \bar{n}_{\mathrm{H},3}^{1/2}$ cm^{-2}, and the magnetic field is $B = 14 \bar{n}_{\mathrm{H},3}^{1/2}$ μG. Much of the unbound molecular gas in the Galaxy satisfies the turbulence-dominated linewidth-size relation (Falgarone et al. 2009). If the simulated system satisfies this relation, then the density is $\bar{n}_{\mathrm{H}} = 370$ cm^{-3} from equation (60), and correspondingly the size of the simulation box is $\ell_0 = 0.4$ pc, the mass is $M_0 = 0.9 M_\odot$, the column is $N_{\mathrm{H}} = 4.7 \times 10^{20}$ cm^{-2}, and the magnetic field is $B = 8.7$ μG.

Next, consider the simulations with $R_{\mathrm{AD}}(\ell_0) = 12, 120$. For these runs, the implied virial parameter is less than unity for the fiducial values of the ionization and coupling parameters. If $\gamma_{\mathrm{AD}}^* \chi_i^*$ is as close as possible to its fiducial value, then the inequality in equation (64) becomes an equality, and equations (47), (49), and (50) imply $\ell_0 = 1.3 \bar{n}_{\mathrm{H},3}^{-1/2}$ pc, $M_0 = 82 \bar{n}_{\mathrm{H},3}^{-1/2} M_\odot$, and $N_{\mathrm{H}} = 4.1 \times 10^{21} \bar{n}_{\mathrm{H},3}^{1/2}$ cm^{-2}. These conditions correspond to $\alpha_{\mathrm{vir}} = 1$, so the systems are on the virialized linewidth-size relation. As remarked above, the virialized linewidth-size relation applies when the density and column density are large, $\bar{n}_{\mathrm{H}} \gtrsim \bar{n}_{\mathrm{LWS}} = 1.1 \times 10^4$ cm^{-3} and $N_{\mathrm{H}} \gtrsim N_{\mathrm{LWS}} = 1.3 \times 10^{22}$ cm^{-2}. Correspondingly, the

size of the system is $\ell_0 \lesssim 0.4$ pc the mass is $M_0 \lesssim M_{\mathrm{LWS}} = 25 M_\odot$, and the magnetic field is $B \gtrsim 50$ μG.

In sum, the systems we have simulated are relatively small, with $\ell_0 \lesssim 1/\bar{n}_{\mathrm{H},3}^{1/2}$ pc (eqs. 47 and 52) and $M_0 \lesssim 100/\bar{n}_{\mathrm{H},3}^{1/2} M_\odot$ (eq. 49). If the system being simulated lies on the linewidth-size relation, then its mass is $M \lesssim M_{\mathrm{LWS}} = 25 M_\odot$. As shown in §A.2.3, this inequality also holds if the system has a linewidth greater than that given by the linewidth-size relation. Similarly, equation (47) shows that the size of the system decreases with σ_{pc}^*; as a result, if the system being simulated lies on or above the linewidth-size relation, then its size is no larger than the size corresponding to the turbulence-dominated linewidth-size relation, $\ell_0 \lesssim 0.4$ pc. Reference to equations (47) and (49) shows that simulations of larger regions would require higher Mach numbers, given that the Alfvén Mach number is observed to be of order unity.

6. CONCLUSIONS

Ambipolar diffusion is a key process in molecular clouds since it redistributes magnetic flux and damps waves. The importance of ambipolar diffusion in a turbulent medium on a length scale ℓ and velocity disperion v is governed by the AD Reynolds number $R_{\mathrm{AD}} = \ell/\ell_{\mathrm{AD}}$, where $\ell_{\mathrm{AD}} = v_A^2 t_{ni}/v$ is the length scale over which the magnetic field must vary in order to have a drift velocity v between the neutrals and ions (Zweibel & Brandenburg 1997; Zweibel 2002). [Note that R_{AD} is useful in describing ambipolar diffusion whenever the velocity field includes a significant turbulent component; it is not useful for non-turbulent, AD-driven gravitational collapse (Mouschovias 1987) or C-shocks (Draine 1980), where R_{AD} is of order unity.] We have carried out two-fluid simulations of isothermal, turbulent boxes using the code ZEUS MPAD (described in LMK) at a resolution of 512^3 for AD Reynolds numbers ranging from $R_{\mathrm{AD}} = 0.12$ to $R_{\mathrm{AD}} = 1200$, plus a simulation with ideal MHD. The resolution we have used is sufficient to resolve the sonic length within the inertial range, permitting accurate simulations for our $\mathcal{M} = 3$ calculations. The mean Mach numbers were fixed at $\mathcal{M} = 3$ and $\mathcal{M}_A = 0.67$, corresponding to a plasma-β parameter $\beta = 0.1$. The purpose of our simulations was to determine how the properties of the clumps formed in molecular clouds depend on $R_{\mathrm{AD}}(\ell_0)$. One of the simulations (with $R_{\mathrm{AD}}(\ell_0) = 12$) was in the middle of the observed range of the observed values of the AD Reynolds number; two of the simulations (those with $R_{\mathrm{AD}}(\ell_0) - 1.2$ and 120) were somewhat below and above the observed values of $R_{\mathrm{AD}}(\ell_0)$; and the remaining two simulations, with $R_{\mathrm{AD}}(\ell_0) = 0.12$ and 1200, were designed to show the transition to hydrodynamics and ideal MHD, respectively. In order to carry out these simulations, we used the Heavy Ion Approximation with an ionized mass fraction of 10^{-2} (LMK) to represent physical systems with actual ionized mass fractions $\sim 10^{-6}$. We validated our simulations with convergence studies at lower resolution. The power spectra in our simulations show that the inertial range of our simulations extends down to a length scale $\ell_0/20$, which is comparable to the sonic length; it is important to resolve the sonic length in simulations of turbulent boxes since the density has significant fluctuations on larger scales. Our principal conclusions are:

1. Values of the AD Reynolds number R_{AD} in a sample of 15 molecular clumps with measured magnetic fields (Crutcher 1999) range from 3 to 73; the logarithmic mean value is 17. Omitting one outlier, the clumps with upper limits on the magnetic field have an average lower limit of $\langle R_{AD}\rangle_{\log} > 18$. The predicted value of the AD Reynolds number for self-gravitating molecular clouds and clumps with the fiducial ionization is $R_{AD} \simeq 20$, in excellent agreement with observation.

2. Several regimes of ambipolar diffusion can be identified, depending on the ratio of the flow time, t_f, to the ion-neutral collision time, t_{in}, and the neutral-ion collision time, t_{ni}: (I) ideal MHD ($t_f/t_{ni} \to \infty$, corresponding to $R_{AD} \to \infty$ for a given value of $\mathcal{M}_A$); (II) standard ambipolar diffusion, with $t_f > t_{ni}$, so that the neutrals and ions are coupled together over a flow time; (III) strong AD ($t_{ni} > t_f > t_{in}$), so that the neutrals are not coupled to the ions over a flow time, but the ions are coupled to the neutrals; (IV) weakly coupled ($t_{in} > t_f$), so that the ions and neutrals behave almost independently over a flow time; and (V) hydrodynamics ($t_f/t_{in} \to 0$ or $\chi_i \to 0$, corresponding to $R_{AD} \to 0$). The molecular clumps in Crutcher's sample are all in the second regime, standard AD.

3. Implied self-gravity: Since the ionization scales approximately as the square root of the density, the ambipolar diffusion time is proportional to the gravitational free-fall time (Mouschovias 1987). As a result, any simulation of ambipolar diffusion has a gravitational virial parameter α_{vir} that is determined by R_{AD}, $\mathcal{M}_A$ and the parameters describing the ion-neutral coupling and the ionization [$\alpha_{vir} \propto (\gamma_{AD}^*\chi_i^*/R_{AD})^2\mathcal{M}_A^4$—eq. 30]. It is not possible to carry out a simulation in which the effects of self-gravity and ambipolar diffusion are varied independently unless the ionization is treated as a free parameter.

4. Clump mass spectrum. Using Clumpfind (Williams, De Geus, & Blitz 1994), we found all the clumps with densities exceeding the mean density in the box. We find that the slope of the higher-mass portion of the resulting clump mass spectrum increases as R_{AD} decreases, which is qualitatively consistent with Padoan et al's (2007) finding that the mass spectrum in hydrodynamic turbulence is significantly steeper than in ideal MHD turbulence. The value of the slope that we find for $R_{AD} = 12$, the case closest to the value observed in molecular clouds, is $\Gamma_{fit} = 1.43 \pm 0.10$, which is consistent with the Salpeter value, $\Gamma = 1.35$. The almost-ideal MHD case ($R_{AD} = 1200$) has a slope $\Gamma_{fit} = 1.22 \pm 0.11$, which is marginally consistent with the Salpeter value. We further confirm Padoan et al's (2007) relation between the index of the power spectrum and the slope of the clump mass spectrum in the limiting cases of ideal MHD and near hydrodynamics. However, the value we find for the spectral index in our ideal MHD simulation differs from theirs, presumably because our simulation has lower values

of β and $\mathcal{M}$. This suggests that the IMF in the Padoan & Nordlund (2002); Padoan et al. (2007) turbulent fragmentation model depends on the environment, which could conflict with evidence for an IMF that is approximately universal (see also Ballesteros-Paredes et al. 2006).

5. Ambipolar diffusion affects the mass-to-flux ratio of clumps, even in the absence of self-gravity: The average mass-to-flux ratio $\mu_{\Phi,c}/\mu_{\Phi,0}$ at low R_{AD} is slightly larger than at high R_{AD}, and the dispersion in the values of $\mu_{\Phi,c}/\mu_{\Phi,0}$ for individual clumps at moderate R_{AD} is almost twice that at high R_{AD}.

6. Scaling relations for simulations of isothermal turbulent boxes. A simulation of an isothermal, magnetized, turbulent box is characterized by three dimensional parameters: the size of the box, ℓ_0, the mean density in the box, $\bar{\rho} \propto \bar{n}_H$, and the sound speed, c_s (e.g., Ostriker, Gammie, & Stone 1999). A single simulation with ideal MHD applies to an infinite range of values of each of these dimensional parameters, provided that the dimensionless parameters describing the simulation (in this case, the Mach numbers $\mathcal{M}$ and $\mathcal{M}_A$) are the same (e.g., Padoan & Nordlund 1999). Except in regions of high-mass star formation, molecular gas generally has a temperature $T \sim 10-20$ K, so that c_s is nearly constant; as a result, there are only two dimensional parameters that have a significant variation, ℓ_0 and $\bar{\rho}$. Each physical process that is introduced into the simulation, such as ambipolar diffusion, introduces a dimensionless parameter, such as R_{AD}, which must be fixed for the simulation, thereby reducing the number of scaling parameters by one. For simulations with ambipolar diffusion, the physical parameters describing the system being simulated are characterized by a single dimensional parameter (for constant c_s), which we took to be the mean density (§5.1). Such simulations are intrinsically scale free. Even if one includes self-gravity, then, so long as the ionization scales as $\bar{\chi}_i \propto \bar{n}_H^{-1/2}$, the simulation remains scale free. However, if one further requires that the simulation satisfy an observed linewidth-size relation, then the mean density is determined and there are no independent scaling parameters.

7. Physical parameters associated with the simulations. Two of the simulations we carried out were for the purpose of studying the transition to ideal MHD [$R_{AD}(\ell_0) = 1200$] and to hydrodynamics [$R_{AD}(\ell_0) = 0.12$], so we focus on the remaining three, with $R_{AD}(\ell_0) = 1.2, 12, 120$. As discussed in item (3) above, a simulation of ambipolar diffusion has an associated value of the virial parameter. The virial parameter cannot be significantly less than unity since the self-gravity would induce collapse that would lead to $\alpha_{vir} \sim 1$. This constraint gives a lower bound on the ionization such that $R_{AD}(\ell_0) \lesssim 6.4\gamma_{AD}^*\chi_i^*$. As a result, two of the simulations [$R_{AD}(\ell_0) = 12, 120$] could be realized in nature only if the ionization and/or the ion-neutral coupling constant were larger than the

fiducial values, which correspond to $\gamma_{AD}^* \chi_i^* = 1$. The $R_{AD}(\ell_0) = 1.2$ simulation corresponds to a system in which self-gravity is unimportant (for $\gamma_{AD}^* \chi_i^* = 1$), whereas the $R_{AD}(\ell_0) = 12, 120$ simulations correspond to systems that mostly likely are gravitationally bound (for $\gamma_{AD}^* \chi_i^*$ as close to unity as possible). Because of this constraint and because of the small value of the Mach number we adopted ($\mathcal{M} = 3$), our simulations apply to small regions in molecular clouds, with $\ell_0 \lesssim 1/\bar{n}_{H,3}^{1/2}$ pc and $M_0 \lesssim 100/\bar{n}_{H,3}^{1/2}$ $M_\odot$. If the system being simulated has a velocity dispersion on or above the linewidth-size relation observed in the Galaxy, then the size of the region is $\ell_0 \lesssim 0.4$ pc and the mass is $\lesssim 25 M_\odot$.

8. A general discussion of scaling relations for self-gravitating systems is given in the Appendix. In applying the linewidth-size relation, we follow

Falgarone & McKee (2010) in distinguishing the turbulence-dominated relation from the virialized one.

APPENDIX

SCALING LAWS FOR ISOTHERMAL TURBULENT BOXES

In this Appendix, we give a general discussion of scaling laws for simulations of isothermal, turbulent gases in a box. Although we do not include the effects of self-gravity in the text, we do include it here, so as to make the discussion more generally useful. We focus on molecular gas, since such gas is generally approximately isothermal. Particular scaling relations that have been derived previously are noted (Klessen et al. 2000; Ostriker, Gammie, & Stone 1999; Tilley & Pudritz 2004; Vázquez-Semadeni et al. 2005a, 2008).

In the simplest case in which there is no gravity and the MHD is ideal, a simulation of an isothermal, magnetized, turbulent box is characterized by two dimensionless parameters (Padoan & Nordlund 1999), the 3D sonic Mach number, $\mathcal{M} = 3^{1/2}\sigma_{\rm nt}/c_s$, and the plasma-$\beta$ parameter, $\beta \equiv 8\pi\bar{\rho}c_s^2/B_{\rm rms}^2$. Here $\sigma_{\rm nt}$ is the 1D nonthermal velocity dispersion, c_s the isothermal sound speed, $\bar{\rho}$ the mean mass density and $B_{\rm rms} \equiv \langle B^2 \rangle^{1/2}$ the rms magnetic field. Equivalently, the two parameters can be chosen to be the sonic Mach number and the Alfven Mach number, $\mathcal{M}_A \equiv 3^{1/2}\sigma_{\rm nt}/v_A$, since the plasma-$\beta$ parameter is related to $\mathcal{M}$ and $\mathcal{M}_A$ by

$$\beta = 2\left(\frac{\mathcal{M}_A}{\mathcal{M}}\right)^2. \tag{A1}$$

In general, the Mach numbers, $\mathcal{M}$ and $\mathcal{M}_A$, and the plasma-β parameter are functions of time.

The turbulent box is also characterized by three dimensional parameters: the size of the box, ℓ_0, the mean density in the box, $\bar{\rho} = M_0/\ell_0^3$, where M_0 is the mass in the box, and the isothermal sound speed, c_s (e.g., Ostriker, Gammie, & Stone 1999). In the absence of other physical processes, these parameters can be selected arbitrarily. In other words, a given simulation corresponds to definite values of $\mathcal{M}$ and β, but it can be scaled to arbitrary values of $\bar{\rho}$, ℓ_0, and c_s. However, the introduction of a new physical process, such as self-gravity or ambipolar diffusion, introduces a new dimensional constant and a corresponding new dimensionless parameter, so that the number of independent dimensional parameters is reduced by one. The same reduction occurs if a relation between dimensional parameters is assumed, such as a relation between the size of the box and the mean velocity dispersion (a linewidth-size relation). In many cases, the temperature is tightly constrained, so that in fact there are only two dimensional parameters that can be chosen at will. Hence, if an isothermal system satisfies a linewidth-size relation and is either self-gravitating or subject to ambipolar diffusion, then its velocity scale $c_s \propto T^{1/2}$ is set by the assumed temperature and its size and mean density are determined by dimensionless parameters; in this case a given simulation applies to only a single set of parameters describing the box.

We return to the simplest case in which there is neither self-gravity nor ambipolar diffusion. Interstellar densities are often given in terms of number densities; we use the the density of hydrogen nuclei, $n_H = \rho/\mu_H$, where μ_H is the mass per hydrogen nucleus ($= 2.34 \times 10^{-24}$ g for cosmic abundances). Numerically, we have for the mass, flow time, and column density of the box,

$$M_0 = \bar{\rho}\ell_0^3 = 34.6\bar{n}_{H,3}\ell_{0,\rm pc}^3 \quad M_\odot, \tag{A2}$$

$$t_f \equiv \frac{\ell_0}{v_{\rm rms}} = \frac{\ell_0}{\mathcal{M}c_s} = 5.19 \times 10^6 \left(\frac{\ell_{0,\rm pc}}{\mathcal{M}T_1^{1/2}}\right) \quad \text{yr}, \tag{A3}$$

$$N_{\rm H} = \bar{n}_{\rm H}\ell_0 = 3.09 \times 10^{21} \bar{n}_{\rm H,3}\ell_{0,\,\rm pc} \quad {\rm cm}^{-2}, \tag{A4}$$

where $T_1 \equiv T/(10 {\rm\ K})$ and $c_s = 0.188\,T_1^{1/2}$ km s^{-1} for molecular gas with cosmic abundances. The column density corresponds to a surface density

$$\Sigma = 2.34 \times 10^{-3} N_{\rm H,21} {\rm\ g\ cm}^{-2} = 11.2 N_{\rm H,21} {\rm\ } M_\odot {\rm\ pc}^{-2}, \tag{A5}$$

where $N_{\rm H,21} \equiv N_{\rm H}/(10^{21} {\rm\ H\ cm}^{-2})$. The visual extinction corresponding to this column is $A_V = N_{\rm H,21}\delta$ mag, where δ is the ratio of the extinction per unit mass to the Galactic value. The magnetic field is given by (Ostriker, Gammie, & Stone 1999; note that their β is half the normal value)

$$B_{\rm rms} = \left(\frac{8\pi\bar{\rho}c_s^2}{\beta}\right)^{1/2} = 4.56 \left(\frac{\bar{n}_{\rm H,3}T_1}{\beta}\right)^{1/2} \quad \mu{\rm G}, \tag{A6}$$

$$= 3.23\,(\bar{n}_{\rm H,3}T_1)^{1/2}\frac{\mathcal{M}}{\mathcal{M}_{\rm A}} \quad \mu{\rm G}. \tag{A7}$$

Scaling Relations for MHD Simulations of Turbulent Boxes with Self Gravity

As discussed above, self-gravity introduces an additional dimensionless parameter into a simulation and therefore reduces the number of independent dimensional parameters by one. For the case in which the ionization scales as $\bar{\chi}_i \propto \bar{n}_{\rm H}^{-1/2}$, this reduction is the same as that due to the inclusion of ambipolar diffusion (§2.4); that is, for such an ionization law, simulations with both self gravity and ambipolar diffusion obey the same scaling relations as simulations with only one of these processes. In this section, we first summarize the dimensionless parameters used to characterize turbulent simulations with self gravity. We then describe variants of the Jeans mass that take into account turbulent motions. Finally, scaling laws for self-gravitating systems are given for turbulent boxes ($c_A = c_V = 1$—see eqs 21 and 22). With two dimensional parameters specified—the strength of self gravity and the temperature—there is still one free dimensional parameter; as a result, self-gravitating, magnetized turbulent boxes are scale free.

Dimensionless parameters

There are several equivalent dimensionless parameters that can describe the effects of self-gravity. One is the ratio of the mass to the characteristic mass of a self-gravitating cloud, $c_s^3/(G^3\bar{\rho})^{1/2}$:

$$\mu_0 \equiv \frac{M_0}{c_s^3/(G^{3/2}\bar{\rho}^{1/2})}. \tag{A8}$$

This parameter is related to the mass, length and sound speed by

$$\frac{GM_0/\ell_0}{c_s^2} = \mu_0^{2/3}. \tag{A9}$$

In terms of the free-fall velocity, $v_{\rm ff} \equiv (GM_0/2R)^{1/2}$, we have $\mu_0 = (v_{\rm ff}/c_s)^3$.

Another parameter describing the effects of self-gravity is the number of Jeans lengths in the box (e.g. Ostriker, Gammie, & Stone 1999). The typical Jeans length in the box is $\lambda_{\rm J} = (\pi c_s^2/G\bar{\rho})^{1/2}$, so the number of Jeans lengths in the box is

$$n_{\rm J} \equiv \frac{\ell_0}{\lambda_{\rm J}} = \frac{\mu_0^{1/3}}{\sqrt{\pi}}. \tag{A10}$$

The Jeans mass for the box is usually defined as $M_{\rm J} \equiv \bar{\rho}\lambda_{\rm J}^3$, so that the number of Jeans masses in the box is $M_0/M_{\rm J} = (\ell_0/\lambda_{\rm J})^3 = n_{\rm J}^3$. The corresponding value of μ is $\mu_{\rm J} = M_{\rm J}(G^3\bar{\rho})^{1/2}/c_s^3 = \pi^{3/2} \simeq 5.57$.

A third parameter describing the effects of self-gravity is the virial parameter, which for a spherical cloud of radius R is

$$\alpha_{\rm vir} = \frac{5\sigma^2 R}{GM_0} \tag{A11}$$

(Bertoldi & McKee 1992); here $\sigma^2 = c_s^2 + \sigma_{\rm nt}^2$ is the total 1D velocity dispersion. Self gravity is important for $\alpha_{\rm vir} \simeq 1$ and is unimportant for $\alpha_{\rm vir} \gg 1$. By contrast, μ_0 and n_J can have arbitrary values $\gtrsim 1$ when self gravity is important. In further contrast to μ_0 and n_J, the effects of bulk kinetic energy as well as thermal energy are included in $\alpha_{\rm vir}$. For gas in a box, we define $\alpha_{\rm vir}$ by replacing R by $\ell_0/2$:

$$\alpha_{\rm vir} \equiv \frac{5\sigma^2\ell_0}{2GM_0}, \tag{A12}$$

which is the same as equation (19) in the text. There is a complication here, since $\alpha_{\rm vir}$ is defined with respect to the total velocity dispersion, σ, whereas the linewidth-size relation depends only on the non-thermal velocity dispersion, $\sigma_{\rm nt}$. For $\mathcal{M}^2 \gg 1$, there is no problem, since the two velocity dispersions are nearly the same. Relations involving the

Mach number that do not depend on the linewidth-size relation can be extended to low Mach numbers by redefining $\mathcal{M}$ as $[3(1 + \sigma_{nt}^2/c_s^2)]^{1/2}$; otherwise, such relations are restricted to $\mathcal{M}^2 \gg 1$. Bearing this in mind, we note that equation (A9) implies that $\alpha_{\rm vir}$ is related to the other two parameters by

$$\alpha_{\rm vir} = \frac{5}{6}\left(\frac{\mathcal{M}^2}{\mu_0^{2/3}}\right) = \frac{5}{6\pi}\left(\frac{\mathcal{M}^2}{n_J^2}\right). \tag{A13}$$

Vázquez-Semadeni et al. (2008) derived a similar expression for spherical clouds (their $\alpha = \frac{3}{5}\alpha_{\rm vir}$ and their n_J is R/λ_J, which is half the value we use). The virial parameter is also related to the ratio of the Jeans length to the sonic length (§4.2.1): Equations (35) and (A12) give the relation between the virial parameter and the sonic length as

$$\alpha_{\rm vir} = \frac{5}{6}\frac{c_s^2}{G\bar{\rho}\mathcal{M}^2\ell_s^2} \tag{A14}$$

for $q = \frac{1}{2}$. It follows that the ratio of the Jeans length to the sonic length is

$$\frac{\lambda_J}{\ell_s} = \left(\frac{6\pi\alpha_{\rm vir}}{5}\right)^{1/2}\mathcal{M}. \tag{A15}$$

The parameters that describe the effects of self-gravity determine the ratio of the flow time to the free-fall time, which is

$$t_{\rm ff} = \left(\frac{3\pi}{32G\bar{\rho}}\right)^{1/2} = 1.37 \times 10^6 \bar{n}_{\rm H,3}^{-1/2}\quad\text{yr.} \tag{A16}$$

Relative to the free-fall time, the flow time is

$$\frac{t_f}{t_{\rm ff}} = 1.84\frac{\mu_0^{1/3}}{\mathcal{M}} = 3.27\frac{n_J}{\mathcal{M}} = \frac{1.68}{\alpha_{\rm vir}^{1/2}}. \tag{A17}$$

Variants of the Jeans length and Jeans mass

We can define both large-scale and small-scale variants of the Jeans length and Jeans mass. On large scales, the density is close to the mean, $\bar{\rho}$, but the velocity dispersion is $\sigma \equiv (\sigma_{nt}^2 + c_s^2)^{1/2} = \mathcal{M}c_s/\sqrt{3}$. We therefore define the "turbulent" variants of the Jeans length and Jeans mass by replacing the sound speed c_s with the velocity dispersion σ,

$$\lambda_{J,\,\rm turb} \equiv \left(\frac{\pi\sigma^2}{G\bar{\rho}}\right)^{1/2} = \left(\frac{\mathcal{M}}{\sqrt{3}}\right)\lambda_J, \tag{A18}$$

$$M_{J,\,\rm turb} \equiv \bar{\rho}\lambda_{J,\,\rm turb}^3 = \left(\frac{\mathcal{M}}{\sqrt{3}}\right)^3 M_J. \tag{A19}$$

The corresponding dimensionless quantities are

$$\mu_{\rm turb,\,0} \equiv \frac{M_0}{\sigma^3/(G^{3/2}\bar{\rho}^{1/2})} = \left(\frac{\sqrt{3}}{\mathcal{M}}\right)^3\mu_0, \tag{A20}$$

$$n_{J,\,\rm turb} \equiv \frac{\ell_0}{\lambda_{J,\,\rm turb}} = \left(\frac{\sqrt{3}}{\mathcal{M}}\right)n_J. \tag{A21}$$

Both $\mu_{\rm turb,\,0}$ and $n_{J,\,\rm turb}$ are of order unity when the virial parameter is:

$$\alpha_{\rm vir} = \frac{5}{2\mu_{\rm turb,\,0}^{2/3}} = \frac{5}{2\pi n_{J,\,\rm turb}^2}. \tag{A22}$$

On small scales, however, the velocity dispersion is about equal to the sound speed, c_s, whereas the density can vary over orders of magnitude. In star-forming cores, the typical pressure is the mean turbulent pressure $\bar{\rho}\sigma_{nt}^2$ (Padoan 1995; Krumholz & McKee 2005); for an isothermal gas, this corresponds to a density $\rho_{\rm core} \equiv (\mathcal{M}^2/3)\bar{\rho}$. We now introduce another variant of the Jeans length, the "core Jeans length," $\lambda_{J,\,\rm core}$, in which the velocity dispersion and density are those expected in star-forming cores,

$$\lambda_{J,\,\rm core} = \left(\frac{\pi c_s^2}{G\rho_{\rm core}}\right)^{1/2} = \left(\frac{\pi c_s^2}{G\mathcal{M}^2\bar{\rho}/3}\right)^{1/2} = \left(\frac{\sqrt{3}}{\mathcal{M}}\right)\lambda_J. \tag{A23}$$

For supersonic flows, the core Jeans length is indeed small compared to the turbulent Jeans length, $\lambda_{J,\,\rm core} = (3/\mathcal{M}^2)\lambda_{J,\,\rm turb}$, since it measures the effect of high pressures on thermally supported gas, whereas $\lambda_{J,\,\rm turb}$ measures

the effect of the turbulence on gas at the average density. If self-gravity is important in the turbulent box ($\alpha_{\rm vir} \sim 1$), the core Jeans length is somewhat greater than the sonic length,

$$\frac{\lambda_{\rm J,\,core}}{\ell_s} = \left(\frac{18\pi\alpha_{\rm vir}}{5}\right)^{1/2} = 3.36\alpha_{\rm vir}^{1/2}. \tag{A24}$$

The "core Jeans mass" is smaller than the normal Jeans mass and much smaller than the turbulent Jeans mass,

$$M_{\rm J,\,core} = \rho_{\rm core}\lambda_{\rm J,\,core}^3 = \frac{1}{3}\mathcal{M}^2\bar{\rho}\lambda_{\rm J,\,core}^3 = \left(\frac{\sqrt{3}}{\mathcal{M}}\right)M_{\rm J}. \tag{A25}$$

We expect $M_{\rm J,\,core}$ (or perhaps the somewhat smaller core Bonnor-Ebert mass) to be the typical mass of gravitationally bound cores in a turbulent cloud (Padoan 1995).

Scaling in Terms of the Mean Density

As discussed at the outset, the introduction of an additional physical process, such as self-gravity, reduces the number of independent dimensional parameters to two, which we take to be the density $n_{\rm H}$ and the temperature T. Since the temperature has little variation in molecular clouds, there is effectively only one independent dimensional parameter, $n_{\rm H}$. In terms of $n_{\rm H}$, T and the dimensionless parameters describing the self gravity, the size and mass of the box are then given by

$$\ell_{0,\,{\rm pc}} = 0.488\mu_0^{1/3}\left(\frac{T_1}{\bar{n}_{\rm H,\,3}}\right)^{1/2} = 0.865n_{\rm J}\left(\frac{T_1}{\bar{n}_{\rm H,\,3}}\right)^{1/2} = 0.445\frac{\mathcal{M}}{\alpha_{\rm vir}^{1/2}}\left(\frac{T_1}{\bar{n}_{\rm H,\,3}}\right)^{1/2}, \tag{A26}$$

$$\frac{M_0}{M_\odot} = 4.01\left(\frac{\mu_0 T_1^{3/2}}{\bar{n}_{\rm H,\,3}^{1/2}}\right) = 22.3\left(\frac{n_{\rm J}^3 T_1^{3/2}}{\bar{n}_{\rm H,\,3}^{1/2}}\right) = 3.05\left(\frac{\mathcal{M}^3 T_1^{3/2}}{\alpha_{\rm vir}^{3/2}\bar{n}_{\rm H,\,3}^{1/2}}\right), \tag{A27}$$

$$N_{\rm H,\,21} = 1.50\mu_0^{1/3}(\bar{n}_{\rm H,\,3}T_1)^{1/2} = 2.67n_{\rm J}(\bar{n}_{\rm H,\,3}T_1)^{1/2} = 1.37\left(\frac{\bar{n}_{\rm H,\,3}T_1}{\alpha_{\rm vir}}\right)^{1/2}\mathcal{M}. \tag{A28}$$

Note that the column density is directly proportional to the square root of the thermal pressure in the first two cases, and to the square root of the turbulent pressure, $\bar{\rho}v_{\rm rms}^2 \propto \mathcal{M}^2\bar{n}_{\rm H}T$, in the third case; this is to be expected, since the pressure in a self-gravitating system is proportional to $G\Sigma^2$. The flow time is given by equations (A16) and (A17), the magnetic field by equation (A7) and the ratio of the mass to the magnetic critical mass, $\mu_{\Phi,\,0}$, by equation (27). The scaling relation between the size and density in terms of $n_{\rm J}$ has been given by Ostriker, Gammie, & Stone (1999) and Vázquez-Semadeni et al. (2005a); for the mass in terms of the size and $n_{\rm J}$ by Tilley & Pudritz (2004), although they have a different numerical coefficient than implied by the above relations; and by Klessen et al. (2000) for both the mass and the size in terms of the density for the particular case they consider, which has $n_{\rm J} = 4$.

The Jeans mass and the Bonnor-Ebert mass are

$$M_{\rm J} = 22.3\left(\frac{T_1^{3/2}}{\bar{n}_{\rm H,\,3}^{1/2}}\right) \quad M_\odot, \qquad M_{\rm BE} = 4.74\left(\frac{T_1^{3/2}}{\bar{n}_{\rm H,\,3}^{1/2}}\right) \quad M_\odot, \tag{A29}$$

where for the Jeans mass we have assumed that $\bar{n}_{\rm H}$ is the mean density in the ambient medium, and for the Bonnor-Ebert mass we have assumed that $\bar{n}_{\rm H}$ is the density at the surface of the Bonnor-Ebert sphere. Note that $M_{\rm J}$ and $M_{\rm BE}$ can be expressed in terms of the surface density of the box as, for example, by

$$M_{\rm J} = 3.36\left(\frac{\mu_0^{1/3}T_1^2}{N_{\rm H\,22}}\right) \quad M_\odot, \qquad M_{\rm BE} = 0.713\left(\frac{\mu_0^{1/3}T_1^2}{N_{\rm H,\,22}}\right) \quad M_\odot. \tag{A30}$$

We have changed the normalization of the column density so as to yield values of the Jeans mass and Bonnor-Ebert mass comparable to observed values for $N_{\rm H,22} \equiv N_{\rm H}/(10^{22}~{\rm cm}^{-2}) \sim 1$. The core values are smaller by a factor $\sqrt{3}/\mathcal{M}$. In this case, it is convenient to express the results in terms of the virial parameter of the box,

$$M_{\rm J,\,core} = 5.31\left(\frac{T_1^2}{\alpha_{\rm vir}^{1/2}N_{\rm H,\,22}}\right) \quad M_\odot, \qquad M_{\rm BE,\,core} = 1.13\left(\frac{T_1^2}{\alpha_{\rm vir}^{1/2}N_{\rm H,\,22}}\right) \quad M_\odot. \tag{A31}$$

Note that in both cases, the critical masses have no explicit dependence on the Mach number.

The basic conclusion is that MHD simulations of of self-gravitating, turbulent boxes are scale free; even with the temperature fixed, there is one free parameter, such as the box size or the density, that can be chosen arbitrarily. Similarly, MHD simulations with ambipolar diffusion are scale free, as we have seen in §5. If the ionization scales as $1/\bar{n}_{\rm H}^{1/2}$, then $R_{\rm AD}$ and $\alpha_{\rm vir}$ are directly related (§2.4) and simulations with both ambipolar diffusion and self gravity are also scale free.

Scaling with the Linewidth-Size Relation

Linewidth-Size Relations for Molecular Clouds and Turbulent Boxes

Molecular gas in the Galaxy exhibits a linewidth-size relation in which the velocity dispersion of the gas increases as a power of the physical dimension of the region (Larson 1981). Heyer & Brunt (2004) have shown that this applies within GMCs as well as among different GMCs. The data are consistent with the relation for the 1D velocity dispersion

$$\sigma_{\rm nt} = \sigma_{\rm pc} R_{\rm pc}^q, \tag{A32}$$

with $\sigma_{\rm pc} = 0.72$ km s^{-1} and $q = \frac{1}{2}$ (Solomon et al. 1987; McKee & Ostriker 2007); for these parameters, the Mach number is $\mathcal{M} = 6.63(R_{\rm pc}/T_1)^{1/2}$. Such a relation appears to be satisfied by most molecular gas in the Galaxy; for example, Heyer & Brunt (2004) find $q = 0.49 \pm 0.15$ within individual molecular clouds in their sample, and Falgarone et al. (2009) find that the combined data from several different surveys shows a clear linewidth-size relation, although they do not give a fit. The parameters have different values in regions of high-mass star formation, however: in such regions, $\sigma_{\rm pc} \sim$ a few km s^{-1}, different regions of high-mass star formation do not have line widths that increase as $R^{1/2}$, and it is not known how the velocity dispersion within individual regions scales with size (Plume et al 1997). Nonetheless, equation (A32) appears to be satisfied in these regions to within an order of magnitude.

Mouschovias & Psaltis (1995) and Heyer et al. (2009) have proposed variants of the linewidth-size relation for gas that is gravitationally bound. Falgarone & McKee (2010) have reconciled these *virialized linewidth-size relations* with the classical *turbulence-dominated linewidth-size relation*. Recall that the surface density of the cloud is $\Sigma_0 = M_0/(c_A \ell_0^2)$, where $c_A = (1, \pi/4)$ for a box and a spherical cloud, respectively. The virial parameter (eq. A12) is then

$$\alpha_{\rm vir} \equiv \frac{5\sigma^2}{2G c_A \Sigma_0 \ell_0}, \tag{A33}$$

where we have used the identity symbol to emphasize that this follows directly from the definitions of the quantities involved; there is no physics in this relation. Solving this relation for the velocity dispersion gives

$$\sigma \equiv \left[\frac{\pi}{5} \left(\frac{c_A}{\pi/4} \right) G \alpha_{\rm vir} \Sigma_0 R_0 \right]^{1/2}, \tag{A34}$$

where $R_0 \equiv \ell_0/2$ is the cloud radius. The factor in parentheses with c_A is unity for a spherical cloud. This relation is superficially like the linewidth-size relation in equation (A32), but it is quite different: First, the exponent in the linewidth-size relation, $q \simeq \frac{1}{2}$, follows from observation, whereas that in equation (A34) is $\frac{1}{2}$ by definition, and second the coefficient in relation (A34) depends on the column density. Heyer et al. (2009) inserted the physics into this relation by noting that gravitationally bound clouds have $\alpha_{\rm vir} \simeq 1$. For spherical clouds, they then found

$$\sigma = \left[\frac{\pi}{5} G \Sigma_0 R_0 \right]^{1/2}, \tag{A35}$$

$$= 0.55 (N_{\rm H,22} R_{\rm pc})^{1/2} \quad {\rm km \ s^{-1}} \tag{A36}$$

which we term the virialized linewidth-size relation. They obtained a sample of bound clouds by combining the ^{12}CO data on the Solomon et al. (1987) molecular clouds with data from the higher resolution ^{13}CO data on these clouds from the Galactic Ring Survey (REF). Over a range of surface densities $10 \, M_\odot \ {\rm pc}^{-2} \lesssim \Sigma \lesssim 10^3 \, M_\odot \ {\rm pc}^{-2}$, equation (A36) describes the data well, after a somewhat uncertain correction is made for the cloud masses. Mouschovias & Psaltis (1995) previously found an analogous relation for magnetized clouds with $B\mu_{\Phi,0}$ in place of $N_{\rm H}$ (see eq. 27).

Falgarone & McKee (2010) concluded that non-self gravitating interstellar gas obeys the turbulence-dominated linewidth-size relation given by equation (A32), whereas self-gravitating gas satisfies the virialized linewidth-size relation given by equation (A35). There is a critical surface density that defines the boundary between the turbulent and virialized cases: Equating the velocity dispersions for the two cases gives

$$\Sigma_{\rm LWS} = \frac{5}{\pi G} \left(\frac{\pi/4}{c_A} \right) \left(\frac{\sigma_{\rm pc}^2}{1 \ {\rm pc}} \right), \tag{A37}$$

$$= 192 \left(\frac{\pi/4}{c_A} \right) \sigma_{\rm pc}^{*\,2} \quad M_\odot \ {\rm pc}^2, \tag{A38}$$

where $\sigma_{\rm pc}^* = \sigma_{\rm pc}/(0.72 \ {\rm km \ s^{-1}})$ is normalized to the standard Galactic value (see eq. 55) and $c_A = \pi/4$ for spherical clouds. The corresponding column density is

$$N_{\rm LWS} = 1.71 \times 10^{22} \left(\frac{\pi/4}{c_A} \right) \sigma_{\rm pc}^{*\,2} \quad {\rm cm}^{-2}. \tag{A39}$$

It should be noted that these values for $\Sigma_{\rm LWS}$ and $N_{\rm LWS}$ for spherical clouds are comparable to the mean values for Galactic GMCs found by Solomon et al. (1987), and about twice the mean values found by Heyer et al. (2009).

Regions with $\Sigma \ll \Sigma_{\mathrm{LWS}}$ are dominated by interstellar turbulence, whereas those with $\Sigma \gg \Sigma_{\mathrm{LWS}}$ are dominated by self-gravity and are decoupled from the turbulent cascade in the interstellar medium. The high surface densities of regions of high-mass star formation thus naturally lead to the high velocity dispersions observed there by, for example, Plume et al. (1997). The maximum density for a cloud satisfying the turbulent linewidth-size relation is

$$\bar{n}_{\mathrm{LWS}} = \left(\frac{c_A}{c_V}\right) \frac{N_{\mathrm{LWS}}}{\ell} = 1.83 \times 10^5 \left(\frac{\pi/6}{c_V}\right) \frac{\sigma_{\mathrm{pc}}^{* \, 4}}{\mathcal{M}^2 T_1} \quad \mathrm{cm}^{-3}. \tag{A40}$$

where we used equation (54) to eliminate ℓ and the relations $M \propto c_A N_H \ell^2 = c_V \bar{n}_H \ell^3$ to cover the different geometries. The maximum mass for a cloud satisfying the turbulent linewidth-size relation is

$$M_{\mathrm{LWS}} = 0.311 \left(\frac{\mathcal{M}^4 T_1^2}{\sigma_{\mathrm{pc}}^{* \, 2}}\right) \quad M_\odot, \tag{A41}$$

which is independent of geometry.

Turbulent Boxes with the Turbulence-Dominated Linewidth-Size Relation ($N_H \leq N_{\mathrm{LWS}}$, $c_A = c_V = 1$)

Here we determine the scaling relations for turbulent boxes that satisfy the turbulence-dominated linewidth-size relation

$$\sigma_{\mathrm{nt}} = 0.72 \sigma_{\mathrm{pc}}^* R_{\mathrm{pc}}^{1/2} \quad \mathrm{km \ s}^{-1}. \tag{A42}$$

The Mach number $\mathcal{M}$ and box size ℓ_0 are related by equation (54). As a result, the properties of the turbulent box are given by:

$$\ell_0 = \frac{2}{3} \frac{\mathcal{M}^2 c_s^2}{(\sigma_{\mathrm{pc}}^2 / \, 1\mathrm{pc})} = 0.0455 \left(\frac{\mathcal{M}^2 T_1}{\sigma_{\mathrm{pc}}^{* \, 2}}\right) \quad \mathrm{pc}, \tag{A43}$$

$$t_f = 2.36 \times 10^5 \left(\frac{\mathcal{M} T_1^{1/2}}{\sigma_{\mathrm{pc}}^{* \, 2}}\right) \quad \mathrm{yr}, \tag{A44}$$

$$M_0 = 3.25 \times 10^{-3} \left(\frac{\mathcal{M}^6 \bar{n}_{H,3} T_1^3}{\sigma_{\mathrm{pc}}^{* \, 6}}\right) \quad M_\odot, \tag{A45}$$

$$N_H = 1.40 \times 10^{20} \left(\frac{\mathcal{M}^2 \bar{n}_{H,3} T_1}{\sigma_{\mathrm{pc}}^{* \, 2}}\right) \quad \mathrm{cm}^{-2}. \tag{A46}$$

For simulations that include self-gravity but have surface densities less than the critical one ($\Sigma \leq \Sigma_{\mathrm{LWS}}$), the column density is most simply expressed in terms of the linewidth-size parameter and the virial parameter using equations (A33) and (A43),

$$N_H = \frac{5}{4} \left(\frac{\sigma_{\mathrm{pc}}^2}{1 \ \mathrm{pc}}\right) \frac{1}{G \mu_H \alpha_{\mathrm{vir}}} = 1.34 \times 10^{22} \left(\frac{\sigma_{\mathrm{pc}}^{* \, 2}}{\alpha_{\mathrm{vir}}}\right) \quad \mathrm{cm}^{-2}, \tag{A47}$$

which corresponds to $N_H = N_{\mathrm{LWS}}/\alpha_{\mathrm{vir}}$ for $c_A = 1$ in equation (A39). The scaling for the density can be expressed in terms of the linewidth-size parameter σ_{pc}^* and a parameter describing the self gravity with the aid of equations (A43) and (A26) ,

$$\bar{n}_{H,3} = 115 \left(\frac{\mu_0^{2/3} \sigma_{\mathrm{pc}}^{* \, 4}}{\mathcal{M}^4 T_1}\right) = 361 \left(\frac{n_{\mathrm{J}}^2 \sigma_{\mathrm{pc}}^{* \, 4}}{\mathcal{M}^4 T_1}\right) = 96 \left(\frac{\sigma_{\mathrm{pc}}^{* \, 4}}{\alpha_{\mathrm{vir}} \mathcal{M}^2 T_1}\right). \tag{A48}$$

Comparison with equation (A40) for a box geometry ($c_V = 1$) shows that $\bar{n}_H = n_{\mathrm{LWS}}/\alpha_{\mathrm{vir}}$, where $\alpha_{\mathrm{vir}} \gtrsim 1$. Similarly, equation (A27) implies

$$\frac{M_0}{M_\odot} = 0.374 \left(\frac{\mu_0^{2/3} \mathcal{M}^2 T_1^2}{\sigma_{\mathrm{pc}}^{* \, 2}}\right) = 1.17 \left(\frac{n_{\mathrm{J}}^2 \mathcal{M}^2 T_1^2}{\sigma_{\mathrm{pc}}^{* \, 2}}\right) = 0.311 \left(\frac{\mathcal{M}^4 T_1^2}{\alpha_{\mathrm{vir}} \sigma_{\mathrm{pc}}^{* \, 2}}\right), \tag{A49}$$

so that $M_0 = M_{\mathrm{LWS}}/\alpha_{\mathrm{vir}}$, where M_{LWS} is given in equation (A41). The turbulence-dominated linewidth-size relation does not apply for densities exceeding n_{LWS}, corresponding to column densities $N_H > N_{\mathrm{LWS}}$ and masses $M > M_{\mathrm{LWS}}$, and for that case the scaling is given by the relations in §A.2.3 below.

When expressed in terms of the linewidth-size relation, the core values for the Jeans mass and Bonnor-Ebert mass (eq. A25) are independent of the Mach number,

$$M_{\mathrm{J, core}} = 3.96 \frac{\alpha_{\mathrm{vir}}^{1/2} T_1^2}{\sigma_{\mathrm{pc}}^{* \, 2}} \quad M_\odot, \qquad M_{\mathrm{BE, core}} = 0.84 \frac{\alpha_{\mathrm{vir}}^{1/2} T_1^2}{\sigma_{\mathrm{pc}}^{* \, 2}} \quad M_\odot. \tag{A50}$$

The core Bonnor-Ebert mass is comparable to the typical mass of observed stars, particularly if allowance is made for the fact that only a fraction of the core mass is incorporated into the final star (e.g. Matzner & McKee 2000). These relations can be expressed in terms of the sonic length instead of $\sigma^*_{\rm pc}$ by using equation (39).

In applying these relations to simulations with driven turbulence, it must be kept in mind that the driving generally results in deviations from the linewidth-size relation (A32) on the driving scale. Using the linewidth-size relation to relate simulations to actual systems is therefore best done for cases in which the driving is restricted to large scales; the simulations discussed in the text satisfy this constraint since they are driven over a narrow range of wavenumbers at the largest scale, $1 \leq k \leq k_d$, with the driving wavenumber $k_d = 2$. (Here k is a dimensionless wavenumber that is related to the physical wavenumber $k_{\rm phys}$ by $k \equiv k_{\rm phys}\ell_0/2\pi$; the minimum possible wavenumber is $k = 1$ and the maximum is $\mathcal{N}_g/2$, where $\mathcal{N}_g$ is the number of grid cells in each side of the box.) When the turbulence is driven, one must distinguish between the linewidth-size relation applied to the entire box, and the linewidth-size relation inside the box. In our simulations, the mean Mach number is approximately constant over the range $1 \leq k \leq k_d = 2$. We have chosen to use the full size of the box in relating our simulations to clouds: $\ell_0 = 2R$, where R is the radius of the cloud or of a region inside the cloud. However, in determining properties inside the cloud, such as the sonic length, it is necessary to allow for the fact that the internal linewidth-size relation is normalized approximately to the driving scale. As a result, for $\sigma \propto \ell^{1/2}$, the sonic length is $\ell_s \simeq (\ell_0/k_d)/\mathcal{M}^2$ rather than $\ell_0/\mathcal{M}^2$ (see eq. 36).

General Scaling with the Linewidth-Size Relation

The virialized linewidth-size relation follows from assuming that the virial parameter is unity, so the scaling relations for this case are given by the results in §A.1.3 with $\alpha_{\rm vir} = 1$. To cover both the turbulence-dominated and virialized cases, note that equation (A46) shows that $N_{\rm H} \propto \bar{n}_{\rm H}$ for the turbulence-dominated case ($\alpha_{\rm vir} \gtrsim 1$), corresponding to $\bar{n}_{\rm H} \lesssim \bar{n}_{\rm LWS}$, whereas equation (A28) shows that $N_{\rm H} \propto \bar{n}_{\rm H}^{1/2}$ for $\alpha_{\rm vir} = 1$, corresponding to $\bar{n}_{\rm H} \gtrsim \bar{n}_{\rm LWS}$. As a result, we have

$$N_{\rm H} = N_{\rm LWS} \min \left[\frac{\bar{n}_{\rm H}}{n_{\rm LWS}}, \left(\frac{\bar{n}_{\rm H}}{n_{\rm LWS}} \right)^{1/2} \right] \tag{A51}$$

for the turbulence-dominated and virialized cases, respectively, as can be verified by direct substitution using equations (A28), (A39) and (A40). Similarly one can show that

$$M_0 = M_{\rm LWS} \min \left[\frac{\bar{n}_{\rm H}}{\bar{n}_{\rm LWS}}, \left(\frac{\bar{n}_{\rm LWS}}{\bar{n}_{\rm H}} \right)^{1/2} \right] \tag{A52}$$

with the aid of equations (A27), (A40) and (A41). Note that $M_{\rm LWS}$ is the maximum possible mass for a cloud with a given velocity dispersion, $\sigma \propto \mathcal{M}T^{1/2}$, and linewidth-size coefficient, $\sigma^*_{\rm pc}$ (Falgarone & McKee 2010). Furthermore, for a simulation with a given Mach number, $M_{\rm LWS}$ decreases as $\sigma^*_{\rm pc}$ increases (eq. A41); as a result, $M_{\rm LWS}$ is also the maximum mass of a cloud with a linewidth above the linewidth-size relation. The size of the simulation box is

$$\ell_0 = 0.0455 \left(\frac{\mathcal{M}^2 T_1}{\sigma^{*2}_{\rm pc}} \right) \min \left[1, \left(\frac{n_{\rm LWS}}{\bar{n}_{\rm H}} \right)^{1/2} \right] \quad \text{pc} \tag{A53}$$

based on equation (A26). It must be borne in mind that these equations are based on the mean linewidth-size relation; for a given size and/or surface density, the velocity dispersion can vary by a factor of a few. Thus the virialized linewidth-size relation, which applies to regions with high column densities by definition, correspondingly applies to regions of high density but with sizes and masses that decrease as the column density increases.

Code Units

Numerical codes are generally written in dimensionless form, with masses, lengths and times written in terms of code units, $\tilde{M} = M/M_{\rm code}$, $\tilde{\ell} = \ell/\ell_{\rm code}$, and $\tilde{t} = t/t_{\rm code}$. The code units can be adjusted to fit the problem being simulated. The properties of the box in code units, $\tilde{M}_0 = M_0/M_{\rm code}$ and $\tilde{\ell}_0 = \ell_0/\ell_{\rm code}$, can be selected arbitrarily prior to the simulation (e.g., $\tilde{M}_0 = 8$ and $\tilde{\ell}_0 = 2$), as can the normalized sound speed, $\tilde{c}_s = c_s t_{\rm code}/\ell_{\rm code}$. If there are $\mathcal{N}_g$ grid cells in each side of the simulation box, the grid size is $\Delta\tilde{\ell} = \tilde{\ell}_0/\mathcal{N}_g$. For stationary gas, the time step is $\Delta\tilde{t} = C\Delta\tilde{\ell}/\tilde{c}_s$, where C is the Courant number.

The code unit for length is given by $\ell_{\rm code} = \ell_0/\tilde{\ell}_0$, where ℓ_0 is given by equation (A43) if the typical Galactic linewidth-size relation is adopted, by equation (A26) for a self-gravitating gas, and by equation (47) for a gas undergoing ambipolar diffusion. The corresponding code unit for time is given by $t_{\rm code} = \tilde{c}_s\ell_{\rm code}/c_s$. The code unit for mass is given by $M_{\rm code} = M_0/\tilde{M}_0$, where M_0 is given by equation (A27) for a self-gravitating gas, by equation (A49) for a self-gravitating gas that obeys the linewidth-size relation, and by equation (49) for a gas undergoing ambipolar diffusion.

The gravitational constant in the code is

$$\tilde{G} = \frac{GM_{\rm code}t^2_{\rm code}}{\ell^3_{\rm code}} = \left(\frac{GM_0}{\ell_0 c_s^2} \right) \frac{\tilde{\ell}_0 \tilde{c}_s^2}{\tilde{M}_0} = \frac{\mu_0^{2/3}\tilde{\ell}_0 \tilde{c}_s^2}{\tilde{M}_0}, \tag{A54}$$

from equation (A9). Including the Heavy Ion Approximation ($\tilde{\bar{\chi}}_i = \mathcal{R}\bar{\chi}_i$ and $\tilde{\gamma}_{\mathrm{AD}} \propto \gamma_{\mathrm{AD}}/\mathcal{R}$), the ambipolar diffusion constant in the code is

$$\tilde{\gamma}_{\mathrm{AD}} = \frac{\gamma_{\mathrm{AD}} M_{\mathrm{code}} t_{\mathrm{code}}}{\mathcal{R}\ell_{\mathrm{code}}^3} = \left[\frac{2R_{\mathrm{AD}}(\ell_0)}{\mathcal{R}\bar{\chi}_i \mathcal{M}\beta}\right] \frac{\tilde{c}_s \tilde{\ell}_0^2}{\tilde{M}_0}, \tag{A55}$$

where the second step follows from equation (8). [Keep in mind that $\tilde{\ell}_0$, $\tilde{c}_s$, and $\tilde{M}_0$ are arbitrary; in the simulations described in the text, we have taken $\tilde{\ell}_0 = 2$, $\tilde{c}_s = 0.1$ and $\tilde{\bar{\rho}} = \tilde{M}_0/\tilde{\ell}_0^3 = 1$, so that $\tilde{\gamma}_{\mathrm{AD}} = 0.1 R_{\mathrm{AD}}(\ell_0)/\mathcal{R}\bar{\chi}_i \mathcal{M}\beta$.] So long as the Heavy Ion Approximation is valid, the outcome of a simulation is independent of the value of $\mathcal{R}$ since $\tilde{\gamma}_{\mathrm{AD}}$ always enters in combination with $\tilde{\bar{\chi}}_i = \mathcal{R}\bar{\chi}_i$.

We can now address the issue of scaling in AD simulations when the physical ionization is specified by, for example, the value of χ_i^*. In carrying out a simulation, the ionization in code units, $\tilde{\bar{\chi}}_i = \mathcal{R}\bar{\chi}_i$, must be specified; hence, the physical ionization $\chi_i^* \propto \bar{\chi}_i \propto \mathcal{R}^{-1}$. As noted above, the results of a simulation are independent of $\mathcal{R}$ so long as the Heavy Ion Approximation is valid. Thus, a single simulation provides the results for a family of problems with different degrees of ionization but the same values of $R_{\mathrm{AD}}(\ell_0)$ and c_s; as a result, we can use a single simulation to treat the physically plausible range of ionizations for a given value of $R_{\mathrm{AD}}(\ell_0)$, as discussed in §5.1.

REFERENCES

Adams, F. C. & Shu, F. H. 2007, ApJ, 671, 497
Alves, J., Lombardi, M., & Lada, C. J. 2007, A&A, 462, L17
Arons, J., & Max, C. E. 1975, ApJ, 196, L77
Ballesteros-Paredes, J., Gazol, A., Kim, J., Klessen, R. S., Jappsen, A.-K., & Tejero, E. 2006, ApJ, 637, 384
Ballesteros-Paredes, J., Klessen, R. S., Mac Low, M.-M., & Vazquez-Semadeni, E. 2007, Protostars and Planets V, 63
Barranco, J. A. & Goodman, A. A. 1998, ApJ, 504, 207
Bergin, E. A., Plume, R., Williams, J. P., & Myers, P. C. 1999, ApJ, 512, 724
Bertoldi, F. & McKee, C. F. 1992, ApJ, 395, 140
Burgers, J. M. 1974, The Nonlinear Diffusion Equation (Dordrecht: Reidel)
Caselli, P., Walmsley, C. M., Terzieva, R., & Herbst, E. 1998, ApJ, 499, 234
Crutcher, R.M. 1999, ApJ, 520, 706
Dalgarno, A. 2006, PNAS, 103, 411
Draine, B. T. 1980, ApJ, 241, 1021
Draine, B. T., Roberge, W. G., & Dalgarno, A. 1983, 1983, ApJ, 264, 485
Duffin, D. F. & Pudritz, R. E. 2008, submitted to MNRAS, astro-ph 0810.0299
Falgarone, E., Pety, J., & Hily-Blant, P. 2009, A&A, 507, 355
Falgarone, E., & McKee, C.F. 2010, in preparation
Fatuzzo, M. & Adams, F.C. 2002, ApJ, 570. 210
Fiedler, R. A. & Mouschovias, T. Ch. 1992, ApJ, 391, 199
Fiedler, R. A. & Mouschovias, T. Ch. 1993, ApJ, 415, 680
Gammie, C. F., Lin, Y. T., Stone, J. M., & Ostriker, E. C. 2003, ApJ, 592, 203
Goodman, A. A., Barranco, J. A., Wilner, D. J., & Heyer, M. H. 1998, ApJ, 504, 223
Heiles, C. & Troland, T. H. 2005, ApJ, 624, 773
Hennebelle, P., & Chabrier, G. 2008, ApJ, 684, 395
Hennebelle, P., & Teyssier, R. 2008, A&A, 477, 25
Heyer, M. H. & Brunt, C. M. 2004, ApJ, 615, 45
Heyer, M., Krawczyk, C., Duval, J., & Jackson, J. M. 2009, ApJ, 699, 1092
Iroshnikov, P. S. 1963, AZh, 40, 742 (English transl. Soviet Astron., 7, 566 [1964])
Klessen, R. S., Heitsch, F., & Mac Low, M.-M. 2000, ApJ, 535, 887
Klessen, R. S., & Hennebelle, P. 2009, arXiv:0912.0288
Kraichnan, R. H. 1965, Phys. Fluids, 8, 1385
Krumholz, M. R., McKee, C. F. 2005, ApJ, 630, 250
Kulsrud, R. & Pearce, W. P. 1969, ApJ, 156, 445
Larson, R. B. 1981, MNRAS, 194, 809
Li, P. S., Norman, M. L., Mac Low, M.-M., & Heitsch, F. 2004, ApJ, 605, 818
Li, P. S., McKee, C. F., & Klein, R. I. 2006, ApJ, 653, 1280 (LMK)
Li, P. S., McKee, C. F., Klein, R. I., & Fisher, R. T. 2008, ApJ, 684, 380 (LMKF)
Lizano, S. & Shu, F. H. (1989), ApJ, 342, 834
Mac Low, M.-M., Norman, M. L., Konigl A., & Wardle, M. 1995, ApJ, 442, 726

Mac Low, M.-M. & Smith, M. D. 1997, ApJ, 491, 596
Mac Low, M.-M. 1999, 524, 169
Mac Low, M.-M., & Klessen, R. S. 2004, Reviews of Modern Physics, 76, 125
Matzner, C. D., & McKee, C. F. 2000, ApJ, 545, 364
McKee, C. F. 1989, ApJ, 345, 782
McKee, C. F., & Ostriker, E. C. 2007, ARAA, in press.
Mestel, L., & Spitzer, L. 1956, MNRAS, 116, 503
Mouschovias, T. Ch. 1976, ApJ, 207, 141
Mouschovias, T. Ch. 1977, ApJ, 211, 147
Mouschovias, T. Ch. 1979, ApJ, 228, 475
Mouschovias, T. C. 1987, NATO ASIC Proc. 210: Physical Processes in Interstellar Clouds, 453
Mouschovias, T. C., & Psaltis, D. 1995, ApJ, 444, L105
Mouschovias, T. C., & Spitzer, L., Jr. 1976, ApJ, 210, 326
Myers, P. C., & Khersonsky, V. K. 1995, ApJ, 442, 186
Myers, P. C., & Lazarian, A. 1998, ApJ, 507, L157
Nakano, T., & Nakamura, T. 1978, PASJ, 30, 671
Nakano, T. & Tademaru, E. 1972, ApJ, 173, 87
Nakamura, F. & Li, Z. Y. 2008, ApJ, 687, 354
Onishi, T., Mizuno, A., Kawamura, A., Tachihara, K., & Fukui, Y. 2002, ApJ, 575, 950
Ostriker, E. C., Gammie, C. F., & Stone, J. M. 1999, ApJ, 512, 259
Padoan, P. 1995, MNRAS, 277, 377
Padoan, P., & Nordlund, Å. 1999, ApJ, 526, 279
Padoan, P. & Nordlund, Å. 2002, ApJ, 576, 870
Padoan, P., Willacy, K., Langer, W., & Juvela, M., 2004, ApJ, 614, 203
Padoan, P., Nordlund, Å., Kritsuk, A. G., Norman, M. L., & Li, P. S. 2007, ApJ, 661, 972
Pan, L. & Padoan, P. 2008, submitted, astro-ph 0806.4970
Passot, T., Vázquez-Semadeni, E.,& Pouquet, A. 1995, ApJ, 455, 536
Plume, R., Jaffe, D. T., Evans, N. J., II, Martin-Pintado, J., & Gomez-Gonzalez, J. 1997, ApJ, 476, 730
Shu, F. H. 1983, ApJ, 273, 202
Solomon, P. M., Rivolo, A. R., Barret, J. & Yahil, A. 1987, ApJ, 319, 730
Spitzer, L., Jr. 1968, Diffuse Matter in Space (New York: Interscience)
Tachihara, K., Onishi, T., Mizuno, A., & Fukui, Y. 2002, A&A, 385, 909
Tassis, K. & Mouschovias, T. Ch. 2005, ApJ, 618, 769
Tassis, K. & Mouschovias, T. Ch. 2007, ApJ, 660, 388
Tilley, D. A., & Pudritz, R. E. 2004, MNRAS, 353, 769
Tilley, D. A. & Pudritz, R. E. 2007, MNRAS, 382, 73.
Tomisaka, K., Ikeuchi, S., & Nakamura, T. 1988, ApJ, 335, 239
Tóth, G. 1995, MNRAS, 274, 1002
Troland, T. H., & Crutcher, R. M. 2008, ApJ, 680, 457
Vázquez-Semadeni, E., Ballesteros-Paredes, J., & Klessen, R. S. 2003, ApJ, 585, L131
Vázquez-Semadeni, E., Kim, J., Shadmehri, M., & Ballesteros-Paredes, J. 2005a, ApJ, 618, 344

Vázquez-Semadeni, E., Kim, J., & Ballesteros-Paredes, J. 2005b, ApJ, 630, L49

Vázquez-Semadeni, E., González, R. F., Ballesteros-Paredes, J., Gazol, A., & Kim, J. 2008, MNRAS, 390, 769

Wakelam, V., & Herbst, E. 2008, ApJ, 680, 371

Ward-Thompson, D., André, R., Crutcher, R., Johnstone, D., Onishi, T., WIlson, C. 2007, in Protostars and Planets V, ed. Reipurth, B., Jewitt, D., & Keil, K., p.33

Williams, J. P., De Geus, E. J., & Blitz, L. 1994, ApJ, 428, 693

Williams, J. P., Bergin, E. A., Caselli, P., Myers, P. C., & Plume, R. 1998, ApJ, 503, 689

Williams, J. P., Blitz, L., & McKee, C. F. 2000, in Protostars and Planets IV, ed. V. Mannings, A. P. Boss, & S. S. Russell, p.97

Zuckerman, B., & Evans, N. J. 1974, ApJ, 192, L149

Zuckerman, B., & Palmer, P. 1974, ARA&A, 12, 279

Zweibel, E. G. 2002, ApJ, 567, 962
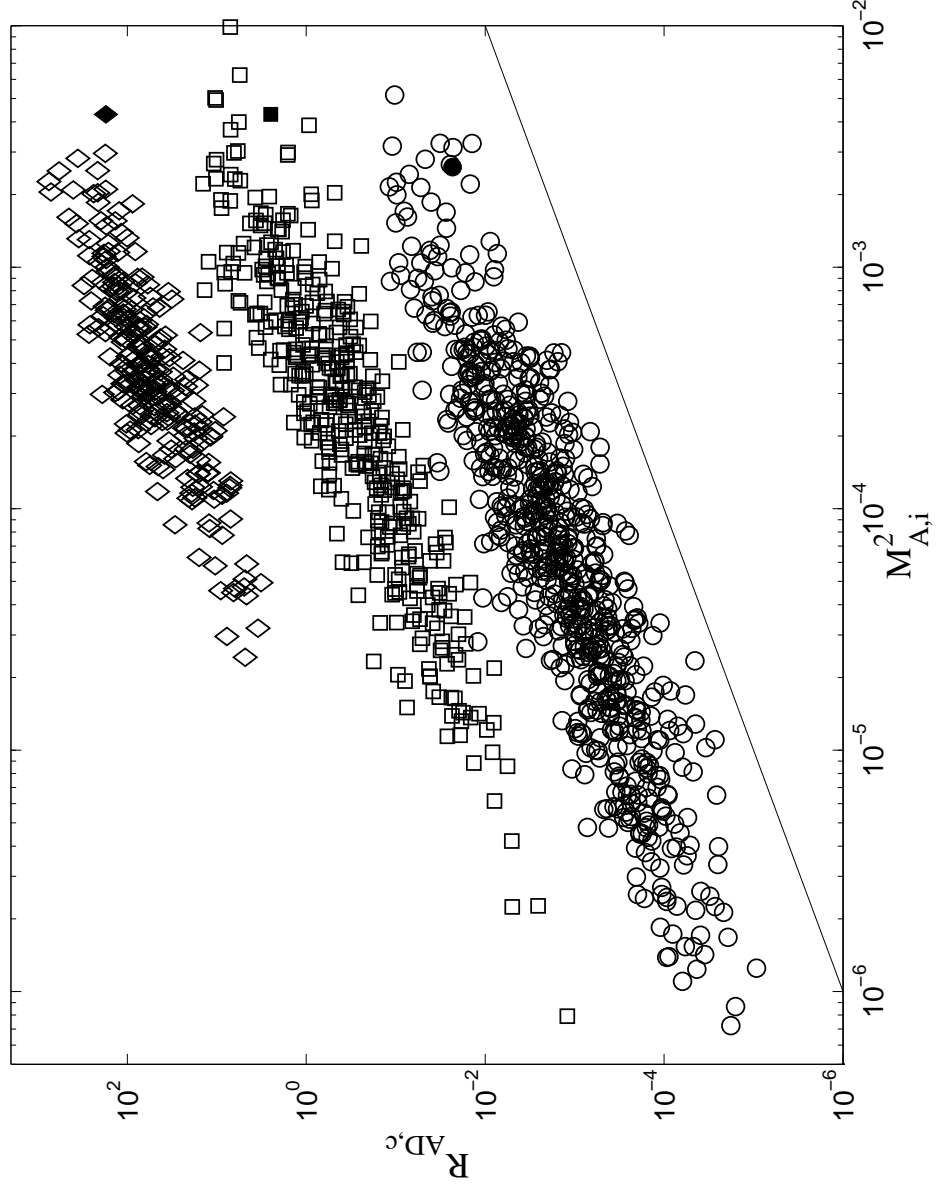
Zweibel, E. G. & Brandenburg, A. 1997, ApJ, 478, 563

FIG. 1.— Clumps' AD Reynolds number, $R_{AD,c}$, versus ion Alfvén Mach number squared, $\mathcal{M}_{Ai}^2$, for models m3c2r-1(circles), m3c2r1(squares), and m3c2r3(diamonds) at the end of the simulation. The straight line shows $R_{AD,c} = \mathcal{M}_{Ai}^2$ and the solid symbols indicate the values of R_{AD} and $\mathcal{M}_{Ai}^2$ for the whole box.
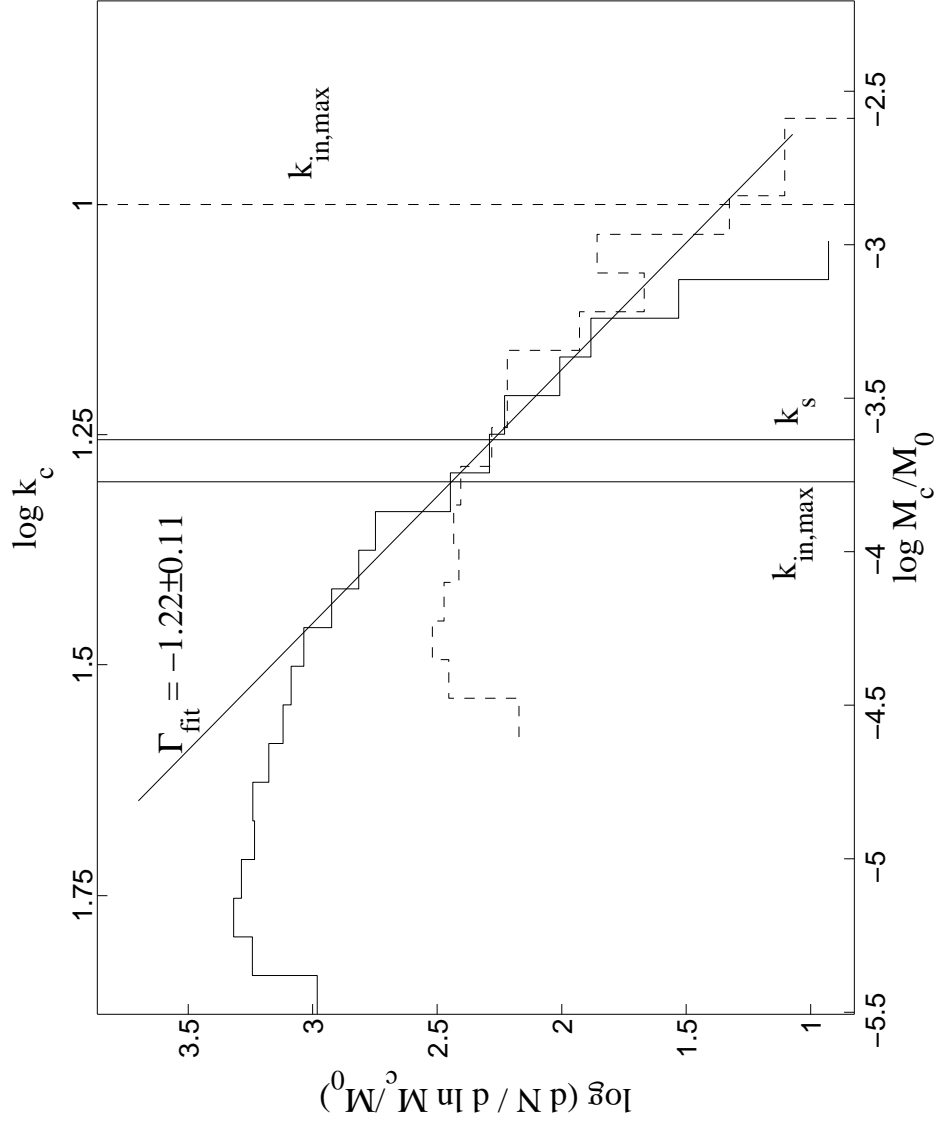
FIG. 2.— Clump mass functions for AD models of $R_{\mathrm{AD}} = 1200$ with grid sizes of 256^3 (dashed line) and 512^3 (m3c2r3, solid line). The sonic wave number, k_s, and the minimum scale of the inertial range, $k_{\mathrm{in, max}}$, for model m3c2r3 are plotted as vertical solid lines; $k_{\mathrm{in, max}}$ for the 256^3 model is plotted as a vertical dashed line. The clump wavenumber k_c based on equation (40) is plotted at the top of the figure for reference; note that k increases to the left. See §4.2.1 for discussion.
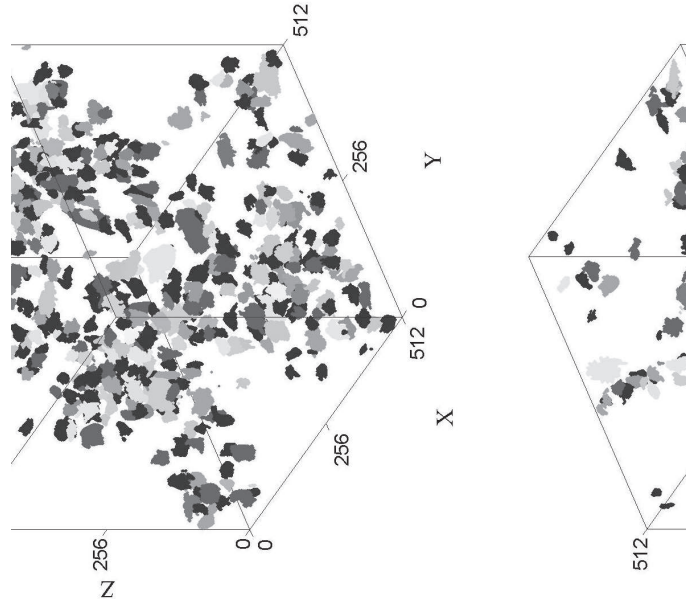
Fig. 3.— 3D spatial distribution of clumps, identified by CLUMPFIND with minimum mean radius of 6 cells, from model m3c2r1. Different gray-scale shadings (different colors in the online version of the paper) are used only to visually separate overlapping individual clumps.
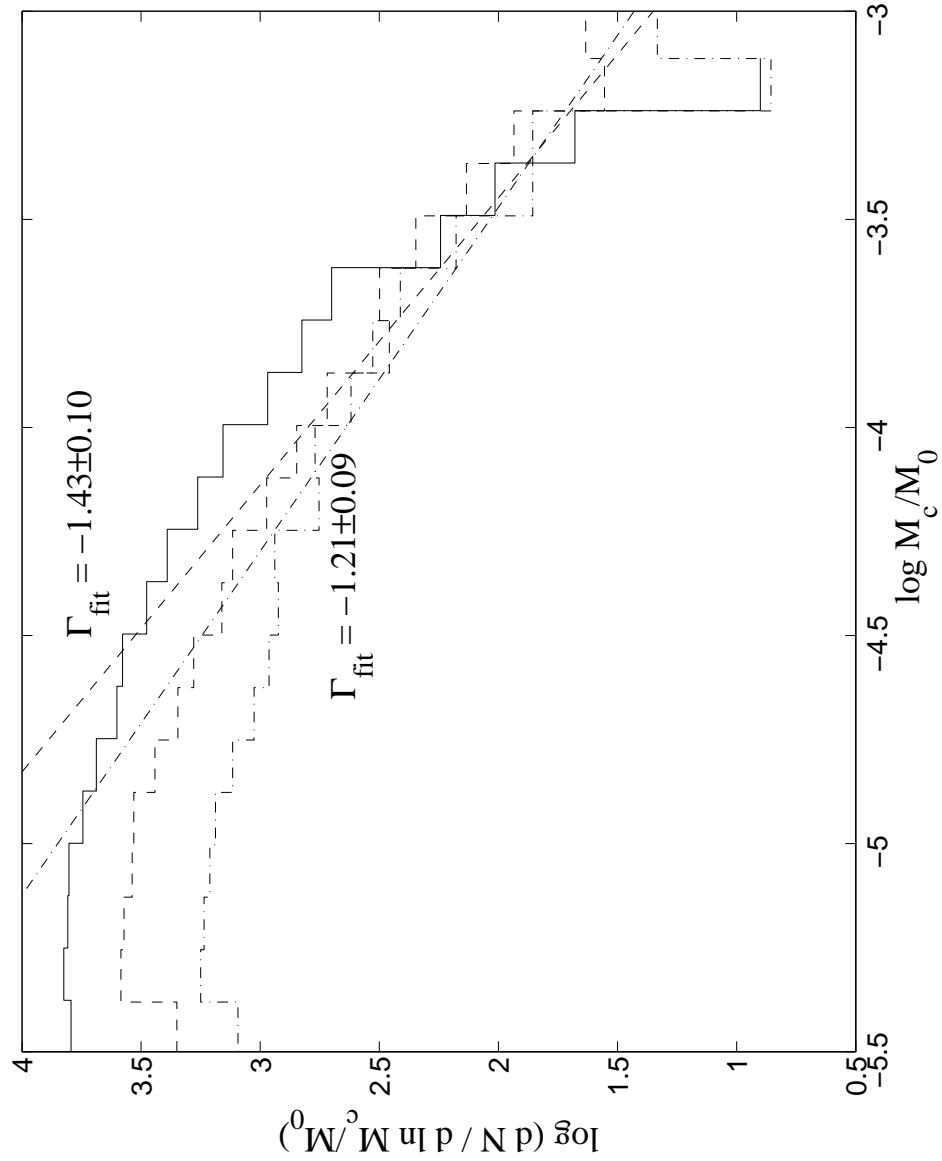
FIG. 4.— Clump mass functions for models m3c2r-1 [$R_{\mathrm{AD}}(\ell_0) = 0.12$; solid line], m3c2r1 [$R_{\mathrm{AD}}(\ell_0) = 12$], and m3i (ideal MHD). The dashed line and dot-dashed line show the best fitting higher-mass slope Γ_{fit} for models m3c2r1 and m3i, respectively. Model m3c2r-1, which has the strongest ambipolar diffusion, has the steepest higher-mass slope (see §4.2.2 for discussion); Model m3i is very similar to model m3c2r3 [$R_{\mathrm{AD}}(\ell_0) = 1200$], which is not shown. All clumps with radius larger than 3 cells are included in the plot.
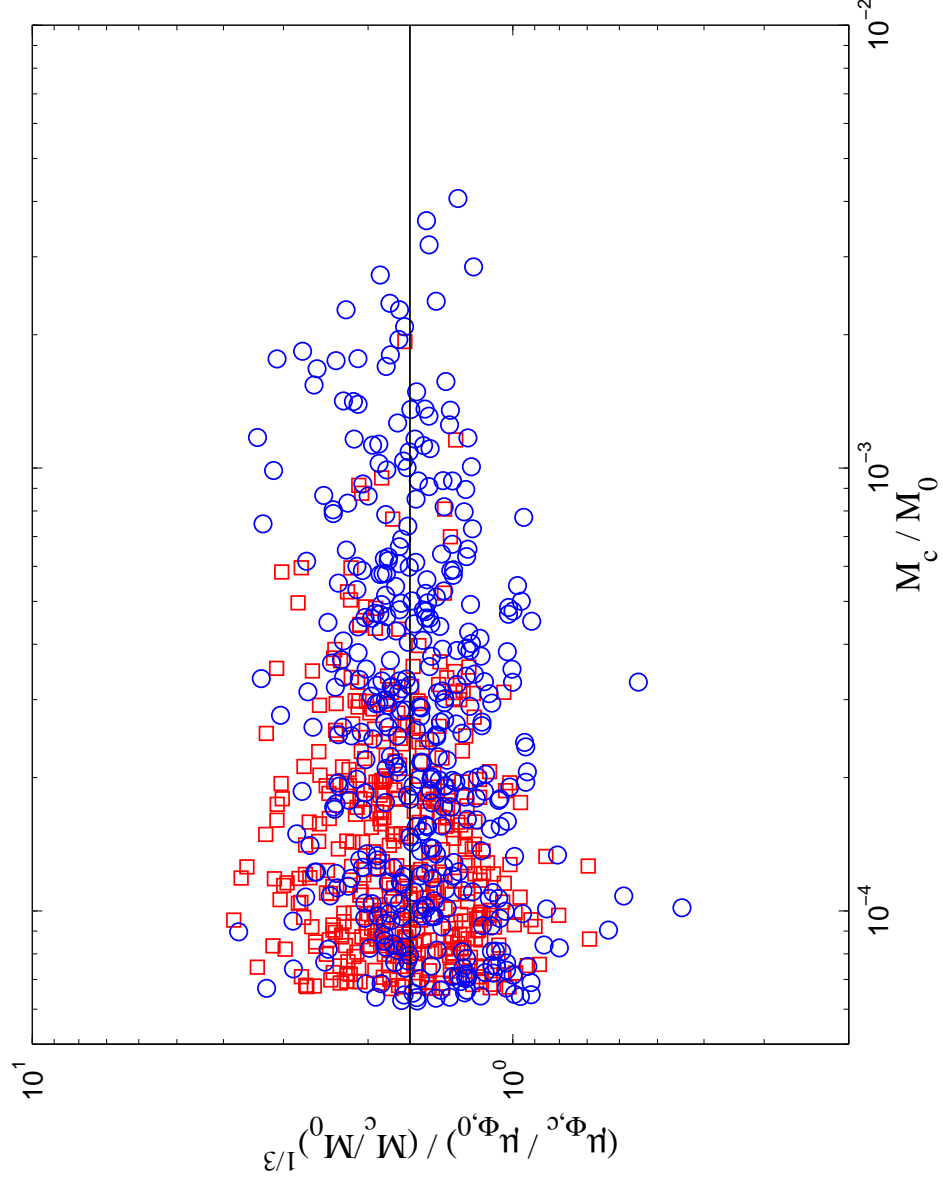
FIG. 5.— Convergence study for the mass-to-flux ratio of the clumps. Values of normalized mass-to-flux ratios of clumps in the $R_{\mathrm{AD}} = 1200$ model are plotted against normalized clump mass, for resolutions of 256^3 (blue cirlces) and 512^3 (red squares; model m3c2r3). By plotting $(\mu_{\Phi,c}/\mu_{\Phi,0})/(M_c/M_0)^{1/3}$ versus M_c/M_0, data points are projected horizontally for easy visual comparison. The straight line shows the mean of the normalized mass-to-flux ratio for elliptical clumps using the mean density and B-field of the clumps from model m3c2r3. See §4.3.1 for discussion.
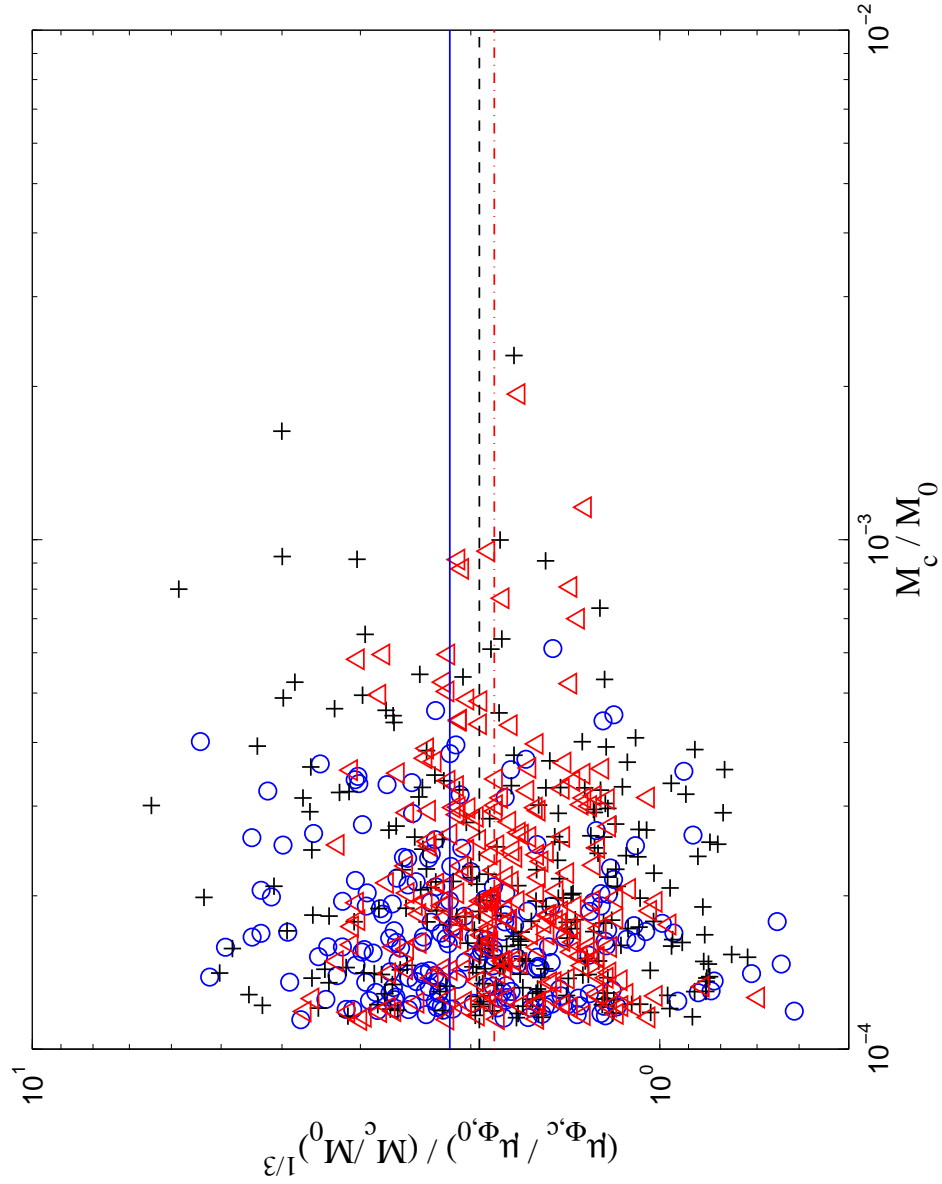
FIG. 6.— Normalized mass-to-flux ratios, $(\mu_{\Phi,c}/\mu_{\Phi,0})/(M_c/M_0)^{1/3}$, of clumps in models m3c2r-1 (blue circles), m3c2r1 (black crosses), and m3c2r3 (red triangles) plotted versus normalized clump mass M_c/M_0. The mean values of $\langle\mu_{\Phi,c}/\mu_{\Phi,0}/(M_c/M_0)^{1/3}\rangle$ for the three models are plotted as the horizontal lines ($R_{\mathrm{AD}}(\ell_0) = 0.12$ blue solid, $R_{\mathrm{AD}}(\ell_0) = 12$ black dashed, and $R_{\mathrm{AD}}(\ell_0) = 1200$ red dot-dashed). The model with the largest value of R_{AD} has a slightly lower average mass-to-flux ratio and a smaller dispersion of the mass-to-flux ratios.
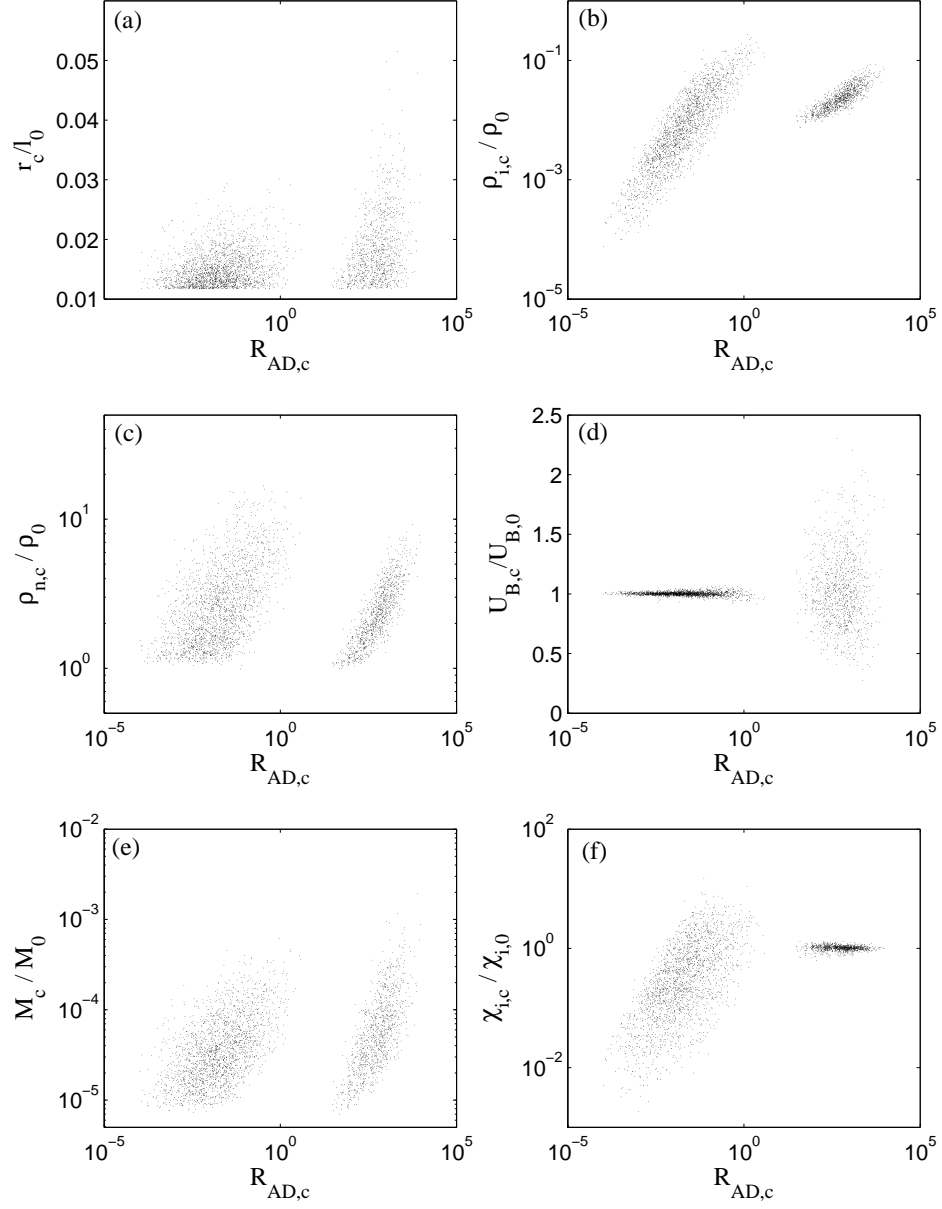
FIG. 7.— Other normalized physical properties of clumps as functions of the AD Reynolds number of the clumps, $R_{\mathrm{AD,c}}$, for the models m3c2r-1 (on the left) and m3c2r3 (on the right): (a) radius, r_c/ℓ_0, (b) ion density; $\langle\rho_i\rangle_c/\bar{\rho}$; (c) neutral density, $\langle\rho_n\rangle_c/\bar{\rho}$; (d) magnetic energy density, $U_{B,c}/U_{B,0}$; (e) clump mass, M_c/M_0; and (f) ionization mass fraction, $\chi_{i,c}/\chi_{i,0}$. See §4.4 for discussion.

McKee, Li, & Klein

TABLE 1
AD Reynolds Number R_{AD} for Observed Molecular Clumps (Crutcher 1999)

Cloud	β	$\log n_2$ (H_2 cm^{-3})	R (pc)	$\mathcal{M}$	$\mathcal{M}_A$	T_k (K)	R_{AD}^a
W3 OH	0.07	6.8	0.02	1.9	0.3	100	3.0
DR 21 OH1	0.21	6.3	0.05	4	1.3	50	37.3
Sgr B2	0.0008	3.4	22	22	0.4	70	10.3
M17 SW	0.008	4.5	1	7	0.5	50	6.3
W3 (main)	0.13	5.5	0.12	4.8	1.2	60	24.1
S106	0.04	5.3	0.07	3.6	0.5	30	3.7
DR 21 OH2	0.41	6	0.05	4	1.8	50	51.5
OMC-1	0.65	5.9	0.05	1.7	1	100	21.9
NGC 2024	0.35	5	0.2	3.7	1.6	25	72.7
S88 B	0.056	3.8	0.7	5.9	1	40	12.9
B1	0.17	4	0.2	3.6	1.1	12	15.7
W49 B	0.024	3	1	5.9	0.6	10	6.3
W22	0.033	3	4	3.5	0.5	10	20.5
W40	0.027	2.7	5	10	1.2	10	42.4
ρ Oph 1	0.42	3.2	0.8	3.5	1.6	25	41.6
OMCN-4	>0.47	6	0.03	2.9	>1.4	35	>30.7
Tau G	>0.042	3	1	5.1	>0.7	10	>9.5
L183	>0.052	3.1	0.3	2.4	>0.4	10	>1.9
L1647	>0.047	3	3	3	>1.4	10	>56.4
ρ Oph 2	>0.14	3	0.9	3.2	>0.8	25	>11.3
TMC-1	>0.063	3	1.9	5.9	>1	10	>31.4
L1495 W	>0.063	3	0.9	3.9	>0.7	10	>9.8
L134	>0.14	3.2	0.3	2.7	>0.7	10	>6.3
TMC-1C	>1.3	4	0.2	2	>1.6	10	>73.0
L1521	>0.13	3	1.2	3.9	>1	10	>27.0
L889	>0.28	3	2.4	7.3	>2.7	13	>191.1
Tau 16	>0.22	3	1.2	3.9	>1.3	10	>45.7

[a] R_{AD} computed using equation (15)

TABLE 2
MODEL PARAMETERS AND REGIMES OF AD

Model[a]	γ_{AD}	$R_{\mathrm{AD}}(\ell_0)$	$R_{\mathrm{AD}}(\ell_0)_t^b$	Regime of AD
m3c2r-1	4	0.12	0.076	III
m3c2r0	40	1.2	0.70	II $\sim$ III
m3c2r1	400	12	10.1	II
m3c2r2	4000	120	103.2	II
m3c2r3	40000	1200	1022	I
m3i	∞	∞		I

[a] Models are labeled as "mxcyrn," where x is the thermal Mach number, $y = |\log \chi_{i0}|$, and $n = \log(R_{\mathrm{AD}}(\ell)/1.2)$. Model "m3i" is an ideal MHD. Model m3c2r0 is the same as model m3c2h in LMKF.
[b] R_{AD} from models using time-dependent ionization (see §3).
[c] Root mean squared (rms) values.

McKee, Li, & Klein

TABLE 3
COMPARISON OF CLUMP PROPERTIES IN MODELS WITH DIFFERENT $R_{\rm AD}$

Model	m3c2r-1	m3c2r1	m3c2r3
$R_{\rm AD}(\ell_0)$	0.12	12	1200
$n_{vn}(k)^a$	1.96 ± 0.02	1.89 ± 0.03	1.48 ± 0.05
$\Gamma^b_{\rm fit}$	-	-1.43 ± 0.10	-1.22 ± 0.11
$\langle \mu_{\Phi,c} \rangle / \mu^c_{\Phi,0}$	0.122 ± 0.004	0.120 ± 0.005	0.111 ± 0.003
$\sigma(\langle \mu_{\Phi,c} \rangle / \mu_{\Phi,0})^d$	0.056	0.074	0.039
$\langle \rho_c \rangle$	6.85 ± 0.24	5.42 ± 0.23	3.19 ± 0.09
$\langle R_{cz}/R_{c,\perp} \rangle$	1.13 ± 0.02	1.15 ± 0.02	2.00 ± 0.05
$\langle r_c \rangle (\text{cell})^e$	9.4 ± 1.1	12 ± 1.5	13.5 ± 1.7
$\langle N_c \rangle \ (d_c > 12 \text{ cells})^f$	698	434	349

[a] Velocity power spectral index of neutral component.
[b] Slope of the ClMF in the inertial range. The data for model m3c2r-1 do not have a single power law over the inertial range.
[c] Clump mass-to-flux ratio normalized by that of the whole box.
[d] Dispersion of clump mass-to-flux ratio normalized by that of the whole box.
[e] Mean radius of clumps in units of number of cells.
[f] Mean number of clumps with diameter larger than 12 cells.